Internal tides responsible for lithogenic inputs along the Iberian continental slope

Simon Barbot[1,1], Marion Lagarde[1,1], Florent Henri Lyard[2,2], Patrick Marsaleix[1,1], Pascale Lherminier[3,3], and Catherine Jeandel[1,4]

[1]LEGOS
[2]Pôle d'Océanographie Côtière de l'Observatoire Midi-Pyrénées (LEGOS)
[3]Ifremer
[4]LEGOS, UMR CNRS 5566, Université Paul Sabatier, CNRS, IRD, CNES

November 30, 2022

Abstract

This study details sediment resuspension due to internal tides (ITs) and the subsequent propagation of suspended particles along and off the Iberian continental slope. Five resuspension sites are identified along the western Iberian shelf slope using a tidal regional model of the Bay of Biscay and Iberian continental shelf. Two sites are sources of lithogenic material, one is a source of biogenic matter, and two are sources of a mixture of both. The potential pathways for particles from the resuspension sites toward the GEOVIDE stations are identified using IBIRYS reanalysis to infer their transport by the ocean circulation. It appears that each station is influenced by a specific pathway and mixed particles from several resuspension sites. This methodology enables us to establish more realistic interpretations of the geochemical in situ observations combining distinct modeling of ITs and oceanic circulation as well as in situ sediment properties. It also reveals that the criticality of the bathymetry slope, commonly used to track the potential occurrence of ITs, is not sufficient to investigate their role in sediment resuspension. An explicit resolution of ITs using a numerical tidal model is required for an exhaustive identification of the resuspension sites.

Internal tides responsible for lithogenic inputs along the Iberian continental slope

Simon Barbot[1], Marion Lagarde[1], Florent Lyard[1], Patrick Marsaleix[1], Pascale Lherminier[2], Catherine Jeandel[1]

[1]LEGOS, Université de Toulouse, CNES, CNRS, IRD, UPS, Toulouse, France
[2]LOPS, Ifremer, Univ. Brest, CNRS, IRD, IUEM, Plouzané, France

Key Points:

- Sites of high bottom tidal velocity along the Iberian continental slope were identified using a semi-realistic internal tides model.
- Sediment resuspension was confirmed on five sites based on earlier sediment surveys and Shields criterion threshold.
- Particle trajectories were proposed based on circulation modeling to improve the interpretation of geochemical tracers measurements.

Corresponding author: Simon Barbot, `simon.barbot@legos.obs-mip.fr`

Abstract

This study proposes new insights for the interpretation of GEOVIDE particle measurements. Potentiel resuspension sites due to internal tides (ITs) have been identified along the western Iberian shelf slope using a tidal regional model. Iberian shelf is mainly a source of lithogenic material whereas Galicia Bank is a source of biogenic matter. The potential pathways for particles from the resuspension sites toward the GEOVIDE stations are identified using IBIRYS reanalysis to infer their transport by the ocean circulation. It appears that each station is influenced by a specific pathway and mixed particles from several resuspension sites.

This methodology reveals that the criticality of the bathymetry slope, commonly used to track resuspension sites from internal waves, is not sufficient to investigate ITs. An explicit resolution of ITs using a numerical tidal model is required for an exhaustive identification of the resuspension sites.

Plain Language Summary

Internal tides are waves with a tidal period generated when tides cross a steep slope of the sea floor. Internal tides then propagate in every stratified layer of the open ocean over hundreds to thousands of kilometers. The encounter of internal tides with underwater relief, either at the generation site or after propagation, results in high bottom friction that enhances sediment resuspension. Evidence of lithogenic particles was found at various depths during the GEOVIDE cruise, from the Iberian continental slope to thousands of kilometers away. The present study identifies the sites where internal tides are responsible for sediment resuspension. Additionally, the oceanic circulation is investigated to establish the trajectories of the resuspended sediment that could explain the GEOVIDE measurements.

Keywords

Internal tides, sediment resuspension, lithogenic particle transport, geochemical tracer, modeling, GEOTRACES

1 Introduction

The GEOVIDE cruise took place in May/June 2014 onboard the R/V "Pourquoi Pas ?" between Lisbon, Greenland, and Newfoundland. This cruise was part of the GEOTRACES program, an international cooperation that aims to study trace elements and their isotopes distributions and cycles in the global ocean. Suspended particles were sampled between the surface and 1000 m at several stations by *in situ* seawater filtration. They were found to have higher Rare Earth Elements (REEs) and iron concentrations closer to the Iberian margin and to contain 40-100% of lithogenic material Gourain et al. (2019), Lagarde et al. (2020). Additionally, a continuous propagation of intermediate nepheloid layers was observed as far as 2000 km away, following isopycnal layers at the following depths: 180, 220, 500 and 800 m (corresponding to potential density anomalies σ = 27.00, 27.05, 27.18 and 27.39 $kg.m^{-3}$ respectively, Fig. 1b, Lagarde et al., 2020). These results suggest intense resuspension along the Iberian continental slope, followed by a transport mechanism allowing the sediment to reach the middle of the Atlantic Ocean as hypothesized by Lagarde et al. (2020). Furthermore, the significant resuspension of particles of strict lithogenic origin leads to the formation of intermediate nepheloid layers when the sediment propagates off-shelf (McCave & Hall, 2002). The presence of nepheloid layers is effectively observed at all depths along the GEOVIDE section, except at 700 m at station 1 (nearest station to the shelf).

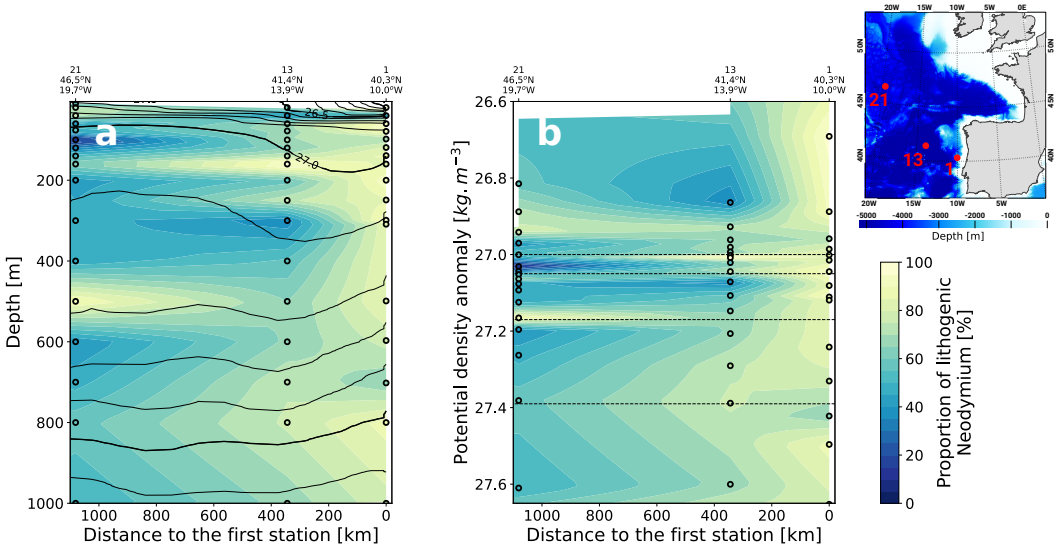

Figure 1. Proportion of lithogenic neodymium in suspended particles (in %) along the 3 first stations over (a) depth and (b) isopycnals. Data from GEOVIDE measurements (black circles) were linearly interpolated with depth (a) and density (b).The solid black lines represent isopycnals of potential density anomaly. The horizontal dashed lines correspond to the isopycnals of the observed nepheloid layers. Station numbers and locations are shown on top of section plots and on the map at the top-right. Data from Lagarde et al. (2020).

The Iberian Peninsula has benefited from a wide coverage of sediment sampling, starting with the surveys of the Dias & Nittrouer (1984), then the OMEX I project and finally the OMEX II-II program. Thanks to the numerous publications of these projects and its database, it is possible to have a complete description of the sediment: grain size spectrum, density and nature. These three properties are necessary to study the resuspension of sediments because a heavier sediment will require a faster current for its resuspension. The nature of the sediment defines whether the sediment was created from submerged organisms (biogenic) or from erosion of the continental crust (lithogenic). Knowledge of the nature of the resuspended sediment is then mandatory to link the resuspension sites to the GEOVIDE measurements (Fig. 1) and better interpret them.

The contribution of internal tides (ITs) and internal solitary waves (ISWs) to sediment resuspension at the margins was demonstrated by lab experiments (Cacchione, 1970), *in situ* measurements (Huthnance, 1989, Jia et al., 2019) and more recently by numerical modeling (Masunaga et al., 2020). Boegman & Stastna (2019) illustrated all the observations of sediment resuspension and transport due to ISWs measurements until then and explained the mechanisms of sediment resuspension by internal waves. Contrasting with the oceanic circulation that transports particles along isopycnals, the turbulence associated with the shoaling of internal waves over the topography enables particles to be transported across isopycnals (Masunaga et al., 2017). ITs and ISWs are generated by distinct forcing that develops a perturbation of the stratification of the water column. They propagate with strong vertical displacements of the isopycnals and enhanced currents.

ISWs have been proposed to explain sediment resuspension along the Iberian shelf (McCave & Hall, 2002, Van Weering et al., 2002, Oliveira et al., 2002, Schmidt et al., 2002, Dias et al., 2002, Quaresma et al., 2007). ISWs are generated by the wind

over a stratified upper ocean or by the tides in a shallow stratified ocean such as a river plume. They can have a large vertical amplitude ($< 200\ m$) and enhanced currents ($< 2\ m.s^{-1}$) but mainly propagate in the first 300 m along the pycnocline (Marin, 2011); therefore, they cannot fully explain the GEOVIDE observations (Fig. 1).

ITs have been observed along the Nazaré canyon without direct evidence of sediment resuspension (Huthnance et al., 2002). Contrary to barotropic tidal currents, which affect the entire water column with a quasi-uniform amplitude, ITs propagate across every stratified layer and the associated currents show a highly variable 3D pattern. Their internal oscillation amplitude is generally weaker than that of ISWs($< 100\ m$ and $< 1\ m.s^{-1}$) but they are highly energetic and constantly generated with a tidal period (de Lavergne et al., 2019). IT energy propagates from IT generation sites in a specific pathway called the wave beam. Effective bottom friction effects are expected where the IT energy flux reaches the seabed, possibly in close vicinity of the generation sites (Garrett & Kunze, 2007, their figure 8). Ribbe & Holloway (2001) showed that IT energy is most efficiently dissipated by friction when the bathymetry slope is parallel to the IT wave beam, a situation called the critical slope which leads to sediment resuspension. The criticality of a bathymetric slope depends on stratification and the tidal period. Its temporal variability is only controlled by the temporal variability of the stratification. This simple criterion is widely used in the geochemical community to identify potential resuspension sites due to the presence of ITs or ISWs at those sites (de Madron et al., 1999, Cacchione et al., 2002, Puig et al., 2004, Lam et al., 2020). ISWs are more randomly generated than ITs, so such a criterion is still valid. However, this approach gives no information on the occurrence of ITs crossing the slope.

The full signal of ITs off-shelf is not easily observed because of their short periods, 3D propagation pattern, and wavelengths of several tens of kilometers. Considering both barotropic and baroclinic tides in circulation models is likely to raise numerical difficulties, such as stability or spurious long-term erosion of the stratification due to strong currents. To date, these processes have been simulated at shelf-scale (tens to hundreds of kilometers) focusing on shallow waters but rarely at wider scales to focus on intermediate sediment resuspension and transport. Molinas et al. (2020) used a tidal regional model to investigate the IT residual currents influencing particle transport over the Amazon shelf but applied their calculation to the shelf only and did not consider the slope and the area further offshore. Masunaga et al. (2020) used a tidal regional model with idealized bathymetry coupled with a sediment model to quantify sediment resuspension and the transport of particles associated with ITs. However, their study did not compare the transport of particles due to ITs to that due to oceanic circulation.

In this context, our purpose is to investigate how ITs trigger sediment resuspension and subsequent transport, as observed along the Iberian margin. First, the 3D hydrodynamic numerical model SYMPHONIE[1] Marsaleix et al. (2008, 2019), forced solely by tides, is used to numerically investigate the bottom current speed and energy budget of ITs. This model was previously deployed in the northeast Atlantic region to study IT dynamics (Pairaud et al., 2008, 2010) and the tidal influences on river plume (Toublanc et al., 2018). The present configuration is based on a high-resolution grid (1 km in the region of interest) and a density field coherent with the GEOVIDE cruise hydrographic conditions. Second, sediment resuspension is investigated using simulated bottom friction and sediment properties. Finally, the consecutive transport of the nepheloid layers is investigated using IBIRYS12[2] (Iberian-Biscay-Irish ocean Reanalysis, hereafter IBIRYS), an operational reanalysis: using 3D hydrodynamic model

[1] `https://sites.google.com/view/symphonieoceanmodel/home`
[2] DOI: `https://doi.org/10.48670/moi-00029`

NEMO (Maraldi et al., 2013), historical simulations have been made using *in situ* measurements to regularly corrected the value of the state variables. This methodology gives realistic insight of the historical state of the ocean for the main physical component (temperature, salinity and velocity). By exploring these processes, this study proposes a mechanistic link between the observed geochemical tracer distributions and the activity of ITs.

2 Internal tide simulation

2.1 SYMPHONIE model configuration

A regional configuration of the SYMPHONIE model, called BOBIBE (Bay of Biscay/Iberian shelf), was set up and 3D tidal simulations were carried out to quantify IT bottom currents and energy dissipation. The BOBIBE configuration uses a realistic bathymetry over a structured grid with a horizontal resolution near 1 km and with 61 vanishing quasi-sigma vertical levels (Estournel et al., 2021). Tides are forced as boundary conditions (with tidal velocity and tidal surface height) and using the astronomical potential. Tidal forcing is based on FES2014b atlas (Lyard et al., 2021) for the M2, S2, K1 and O1 tidal harmonics. These tidal harmonics are selected because they have the largest amplitudes in the studied area and can be separated by harmonic analysis over 15 days. A one-dimensional vertical density profile, representative of the GEOVIDE cruise section, is uniformly prescribed and maintained over the domain. The ocean atmosphere fluxes are disabled preventing any density-driven or wind-driven circulation in the simulation. Further details about the configuration can be found in Supporting Information Text S2.

This IT-dedicated configuration allows the development of a stable IT regime and thus provides a more precise harmonic analysis to extract ITs. The spectral properties (amplitude and phase lag) are extracted from the simulation using harmonic analysis over one month of simulation after 15 days of spinup. To separate the barotropic tides from ITs, the results are projected over the first ten vertical modes based on the mean stratification after spinup. The diagnostics of IT generation and energy flux calculations are based on this modal separation of the results.

2.2 Validation of the simulation

The validation of the BOBIBE simulation focused on the stratification, barotropic velocity, and surface elevation due to ITs. The stratification is compared to that observed during GEOVIDE over the simulation area (average from the first 11 stations). Figure 2a shows that the pycnocline is located at the same depth ($\sim 30\ m$) and despite slight differences at the surface, the stratifications match.

The amplitude of the barotropic velocity was compared to the FES2014b tidal atlas. The major harmonic, M2, is presented in Figure 2b,c (the remaining tidal harmonics can be found in the Supporting Information Fig. S2). The difference is presented in proportion and the white color represents a difference within $\pm 1\%$. The difference between BOBIBE and FES2014b only exceeds 10% at the shelf break and over the Iberian shelf. The barotropic tide is highly sensitive to the bathymetry and energy consumption from IT generation (mostly happening at the shelf break in this area). The bathymetry is better resolved and the IT generation is better constrained in BOBIBE than in FES2014b; therefore, the differences appear reasonable and demonstrate that the overall barotropic tides are well captured.

As explained in the introduction, the measurement of ITs is difficult, making the validation delicate. HRET, one of the best global IT dataset, analyzes 20 years of altimetric surface elevation measurements in order to extract the stationary state

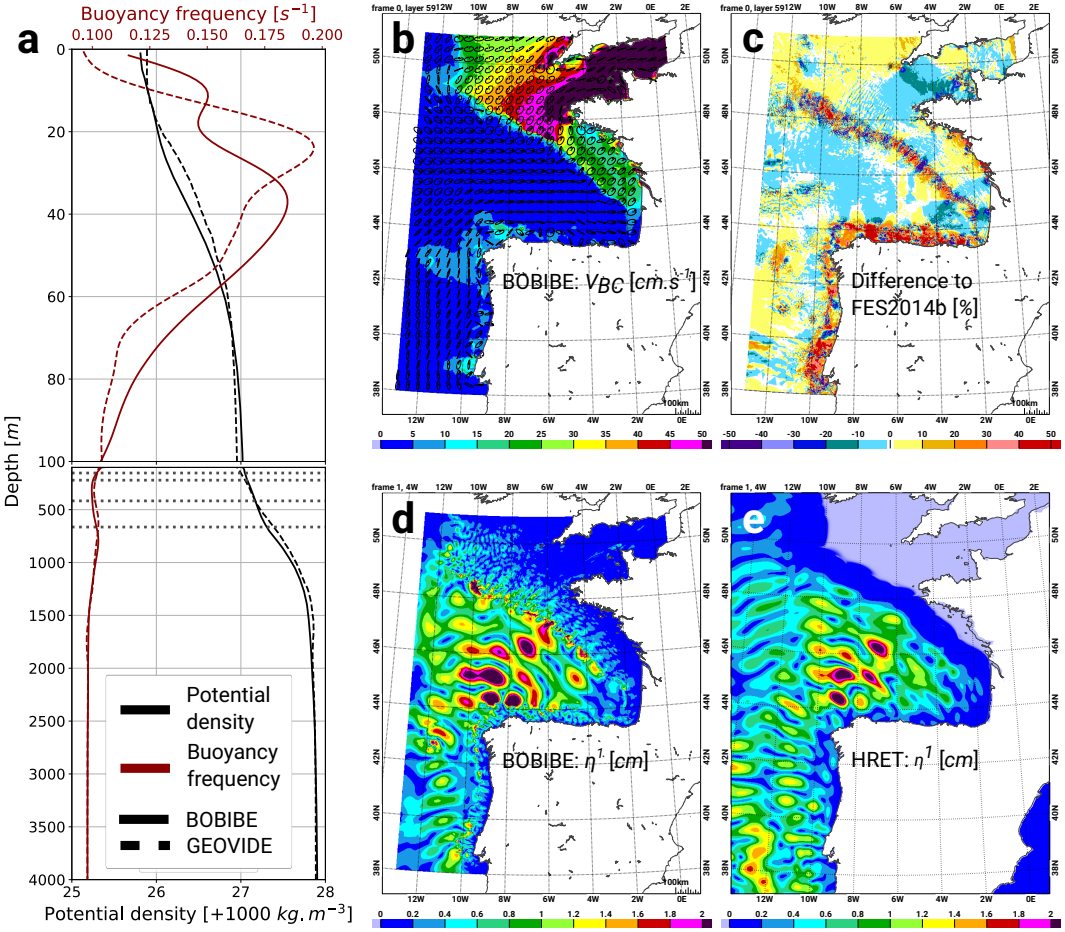

Figure 2. (a) Comparison of the stratification used in BOBIBE and that measured during GEOVIDE (average from the first 11 stations). (b) Amplitude of barotropic velocity for M2 in BOBIBE; and (c) difference to FES2014b atlas in proportion, the white color represents a difference within ±1%. (d) Elevation amplitude of the first baroclinic mode for M2 in BOBIBE; and (e) stationary signal of ITs from HRET. The horizontal dashed lines in (a) correspond to the depths of the observed nepheloid layers.

of ITs globally over different tidal harmonics (Zaron, 2019). The spatial sampling of long-term altimetry (1 Hz data) cannot resolve the IT higher modes, so we choose to compare HRET to the first mode of the BOBIBE simulation. The comparison with M2 is presented in Figure 2d,e; the remaining tidal harmonics can be found in the Supporting Information Fig. S3). The amplitude pattern of ITs is highly similar within the center of the Bay of Biscay but stronger over the Galicia Bank and weaker at the southwest of the domain. HRET uses the hypothesis that ITs are propagating like plane waves to better constrain IT mapping. Such hypothesis appears relevant for large shelf breaks or ridges but is inappropriate for an isolated seamount like the Galicia Bank, where IT propagation is more concentric. At the southwest of the domain, HRET seems to capture the northward ITs generated at the Gorringe Bank, which are not included in the BOBIBE domain.

2.3 Internal tide generation and propagation

Based on the method described in Buijsman et al. (2017), IT energetics are investigated using two quantities: the energy flux (F_{BC}) and the conversion rate (CRV). CRV corresponds to the energy of barotropic tide (BT) converted to baroclinic tide (BC) at the sea floor. Positive CVR values refer to IT generation zones, while negative values refer to a sink of IT energy. Sink zones may correspond to the shoaling of ITs over the bathymetry and could be associated with sediment resuspension. In addition, IT energy fluxes enable the tracking of IT propagation from their generation site to their sink.

F_{BC} and CRV are defined by the following equations:

$$F_{BC} = \int_b^0 \nabla_h \cdot \langle p_{BC} V_{BC} \rangle \, dz \tag{1}$$

$$CVR = \nabla_h \cdot \langle p_{BC}^b V_{BT}^b \rangle \tag{2}$$

with p is the pressure and V is the current velocity, $\langle\rangle$ indicates that the quantities are averaged along the considered tidal period, ∇_h refers to the horizontal gradient and b refers to the sea floor.

Figure 3a shows the IT energy budget and identifies several generation sites with a complex energy propagation. Along the Iberian peninsula, the major generation sites are La Coruña shelf (43^oN,9^oW), the Galicia Bank (43^oN,12^oW) and the Estremadura Spur shelf (39^oN,10^oW). In some areas, the ITs do not propagate and sink locally (shading arrows).

As explained in the introduction, the criticality of the bathymetric slope is widely used to investigate the potential of sediment resuspension from internal waves. The criticality is expressed by the ratio of bathymetric slope over IT wave beam angle (Supporting Information Text S1), whose values of ~ 1 indicate critical slopes (Fig. 3b). We observe that most shelf breaks present critical slopes (from 400 m to 2000 m) that could trigger sediment resuspension. We will now compare this static methodology, only based on the bathymetry and density profile, to a more dynamical methodology involving the current velocity due to ITs.

3 Sediment resuspension triggered by internal tides

3.1 Internal tide bottom friction

To determine where ITs can trigger sediment resuspension, examining the conversion rate is not sufficient because we need to study the kinetic energy applied to the sea floor: the bottom shear stress (or bottom friction). This variable (τ_b) is calculated

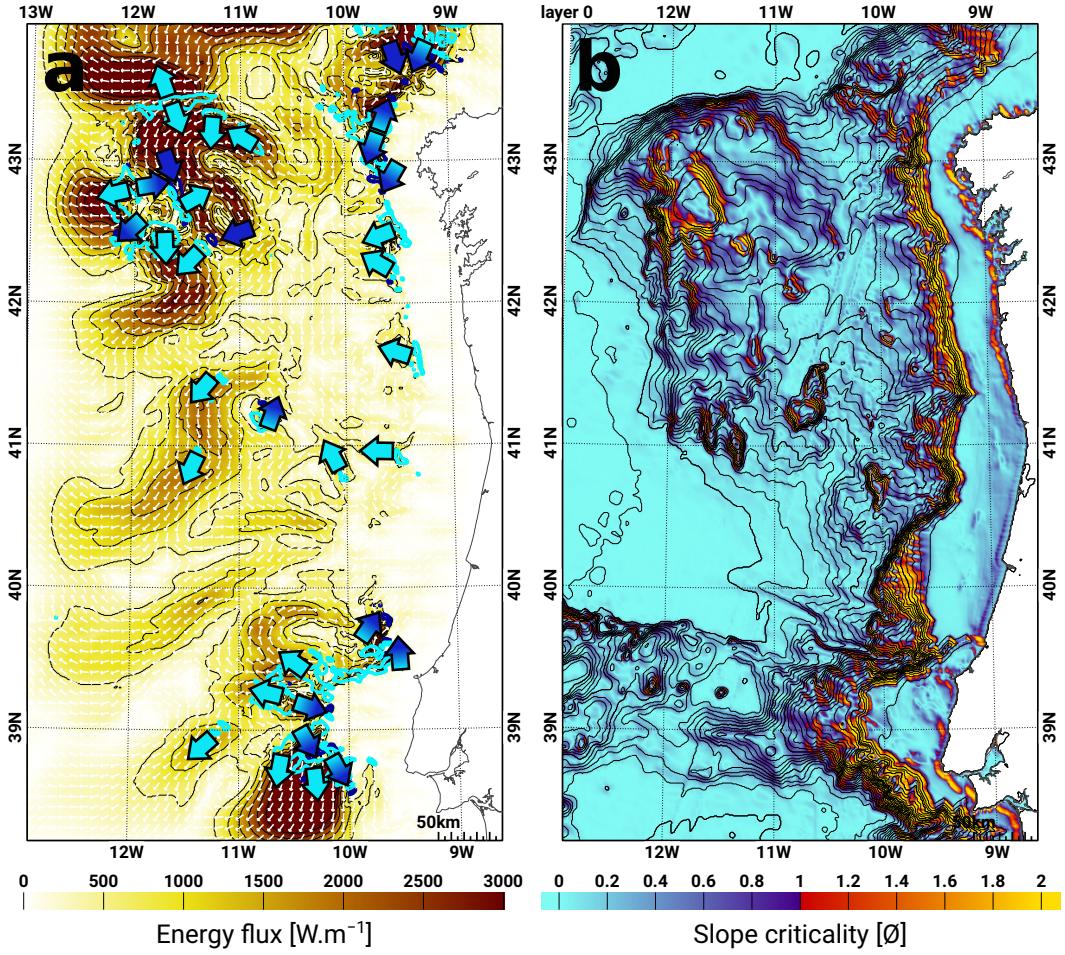

Figure 3. (a) Internal tide energy flux vertically integrated ($W.m^{-1}$) and conversion rate (cyan contours for generation and dark blue contours for sink). The cyan arrows refer to IT generation; the dark blue arrows refer to IT sinks, shading arrows refer to generated and locally dissipated ITs. (b) Ratio between the topography slope and the angle of the IT wave beam for diurnal tidal harmonics (based on M2). Values equal to 1 indicate critical slope areas; values $<$ 1 refer to transmissive slopes (subcritical); and values $>$ 1 refer to reflective slopes (supercritical).

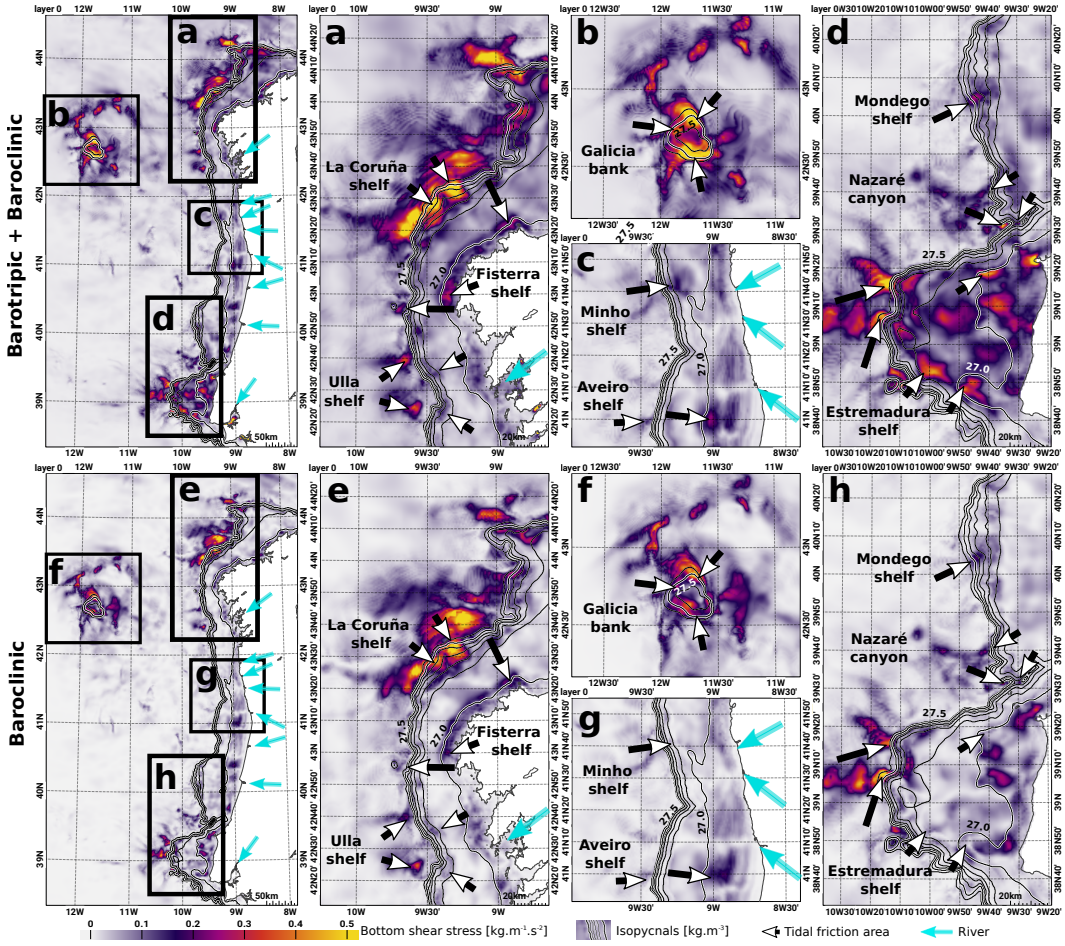

Figure 4. Total (top) and baroclinic (bottom) maximum tidal bottom shear stress from M2, S2, N2, K1 and O1 tidal harmonics over the Iberian continental shelf: (a,e) the northern shelf, (b,f) the Galicia Bank, (c,g) the central shelf and (d,h) the Southern shelf shelf. The isopycnals reflect the potential density at the bottom and highlight the range of the GEOVIDE particle measurements (Fig. 1).The black and white arrows highlight the potential areas of high bottom friction within the isopycnals range considered. The cyan arrows show the rivers bringing lithogenic particles and sediment.

using the equation encoded in the model:

$$\tau_b = \rho V_*^2 = \rho C_D V^2 \tag{3}$$

where ρ is the sea water density, V_* is the friction velocity, C_D is the quadratic friction coefficient and V is the velocity at the vertical mid-position of the bottom layer. C_D is calculated in BOBIBE simulation using the following equation:

$$C_D = \left(\frac{\kappa}{ln\left(\frac{1}{z_0}\frac{h_b}{2}\right)} \right)^2 \tag{4}$$

where κ is the Von Karman constant ($\kappa = 0.4$), z_0 is the bottom roughness and h_b is the thickness of the bottom layer. Equation 4 is valid only if h_b is smaller than the height of the logarithmic velocity profile due to the bottom friction; a condition which is not met in the deep area of the domain. Thus, C_D is forced to be greater than 2.5×10^{-3} as it is commonly done in ocean modeling (Maraldi et al., 2013). The bottom roughness is the scale of unresolved topography at the sea floor, such as sand waves, ripples, or grain size. In the BOBIBE simulation, $z_0 = 1 \times 10^{-3}$ m uniformly over the domain and corresponds to the order of roughness for continental slopes and abyssal plains.

To calculate the maximum τ_b that could occur due to the tides, we calculated $\mathbf{V}$ from the harmonic solutions of the simulation. A tidal prediction of $\mathbf{V}$ from the simulated tidal harmonics (M2, S2, K1 and O1) is made over two months with a time resolution of 30 min. Then, the maximum of V is extracted from this prediction. This method was performed under two scenarios: the total tidal contribution (barotropic and baroclinic) and the baroclinic contribution only (Fig. 4). Nine areas are selected where $\tau_b > 0.1$ $kg.m^{-1}.s^{-1}$, within the range of isopycnals observed during the GEOVIDE cruise (black and white arrows in Fig. 1). All areas are detailed below.

At the northern part of the Iberian peninsula (Fig. 4a,e), 3 areas show intense bottom friction. La Coruña shelf presents a wide area of strong bottom friction over the continental slope which partially corresponds to a critical slope. ITs are mainly generated and dissipated locally (Fig. 3a) but also came from the cap further north (44.1^{o}N-9^{o}W) and from the Bay of Biscay. The Fisterra shelf presents a small sea mount within the continental slope which is crossed by the barotropic tides inducing a very localized bottom friction area. The bottom friction closer to the coast is more likely caused by the ITs from La Coruña shelf, dissipated on a critical slope. Then, the Ulla shelf presents two sites of ITs generation over critical slopes responsible for the bottom friction.

The Galicia Bank (Fig. 4b,f) is a seamount with a summit at 800 m depth with ITs generated on most of its flanks. Other ITs are coming from other sea mounts further north, from the Bay of Biscay and from the Iberian shelves. The maximum bottom friction locations correspond to critical slopes on the flanks of the sea mount but not over its top (Fig. 3b).

At the central part (Fig. 4c,g), Minho and Aveiro shelves are very similar, with barotropic tidal currents coming across steep slopes. But Minho bottom friction is only due to barotropic tides whereas Aveiro one involves ITs generated locally (Fig. 3a and 4g). The maximum bottom friction over these areas is weaker than other sites and Aveiro bottom friction only partially corresponds to a critical slope.

Finally, at the southern part (Fig. 4d,h), three other areas are highlighted. The Mondego shelf is influenced by the ITs from southern shelves, breaking over a supercritical slope. Even with a non-matching criticality, this area shows a medium bottom friction due to ITs. The Nazaré canyon present ITs generation over its flanks with a

strong bottom friction at the bottom of the canyon and some weaker over the northern flanks. These locations partially correspond to critical slopes. The Estremadura Spur shelf is highly influenced by barotropic tides and a lot of the bottom friction is only due to them (Fig. 4h). ITs are generated at the western part over a complex bathymetry with many ITs dissipated locally (Fig. 3a) over critical slopes.

To summarize, the simulation of ITs reveals 9 areas with strong bottom friction that could generate sediment resuspension. Among them, 3 are over critical slopes, 4 others spread over both critical and not critical slopes and 1 occurs over supercritical slopes; 1 area is only due to barotropic tides so the slope criticality is not a concern. In this study, the criterion for sediment resuspension was the maximum tidal bottom friction therefore, the resuspension could occur following the spring-neap tide cycle. The fact that these areas do not strictly correspond to critical slopes increases the number of potential resuspension locations over shelves, offering new perspectives for worldwide sediment tidal resuspension investigations. Hereafter, all these selected areas will be referred to as tidal resuspension sites (TRS).

3.2 Sediment resuspension threshold

After identifying the potential TRS, we investigated whether bottom friction was strong enough to generate sediment resuspension at those sites. The threshold of sediment resuspension can be estimated using the static approach of the Shields criterion. Shields (1936) was one of the first to propose an empirical threshold of sediment resuspension in an adimensional space based on a lab experiment using multiple fluids and sediment. This methodology has been validated for the study of sediment motion in continental shelves by Larsen et al. (1981). This adimensional space uses the Shields parameter (ϑ) to compare bottom friction to sediment properties, and the boundary Reynolds number (Re_*) to describe the turbulence of the flow at the scale of the sediment:

$$\vartheta = \frac{\tau_b}{gd(\rho_S - \rho)} \tag{5}$$

$$Re_* = V_* \frac{d}{\nu} = \sqrt{C_D} \frac{VD}{\nu} \tag{6}$$

where d is the grain diameter of the sediment, ρ is the density of the fluid, ρ_S is the dry bulk density of the sediment and $\nu = 1.41 \times 10^{-6}\ m^2.s^{-1}$ is the kinematic viscosity for sea water.

More recently, analytical Shields curves were formulated for various motion thresholds (motion, rolling, resuspension) and cohesive sediments (silts; Miedema, 2012a,b, 2013). The curve for cohesive sediments has been chosen for the smallest grain size observed to be the most restrictive (7 μm), then the cohesive effect has been added to the rolling threshold. Because the parameters needed to properly generate these curves are missing, custom curves that fit the Shields curves were used.

The sediment properties at each potential TRS are found in the literature, from the closest *in situ* samples (Table 1). The sediment along the Iberian slope have a density from 2.3 $g.cm^{-3}$ to 2.5 $g.cm^{-3}$, whereas the Galicia Bank sediment have a density of 1.7 $g.cm^{-3}$ which greatly affect the relation between (D,$\mathbf{V}$) and (ϑ,Re_*). Thus, for clarity purposes, Galicia Bank is considered separately as well as the TRSs that present silt.

Figure 5 compares the values of ϑ and Re_* at the potential TRS (colored rectangles) to the Shields curves (in black). Cases falling below the rolling curve correspond to steady sediment. Cases falling above the rolling curve but below the resuspension curve correspond to lifted sediment which sink back. Cases falling above every curve are favorable to sediment resuspension, because the sediment is light enough, thin enough or the flow is strong enough (black labels in Fig. 5a). Sediment with cohesive

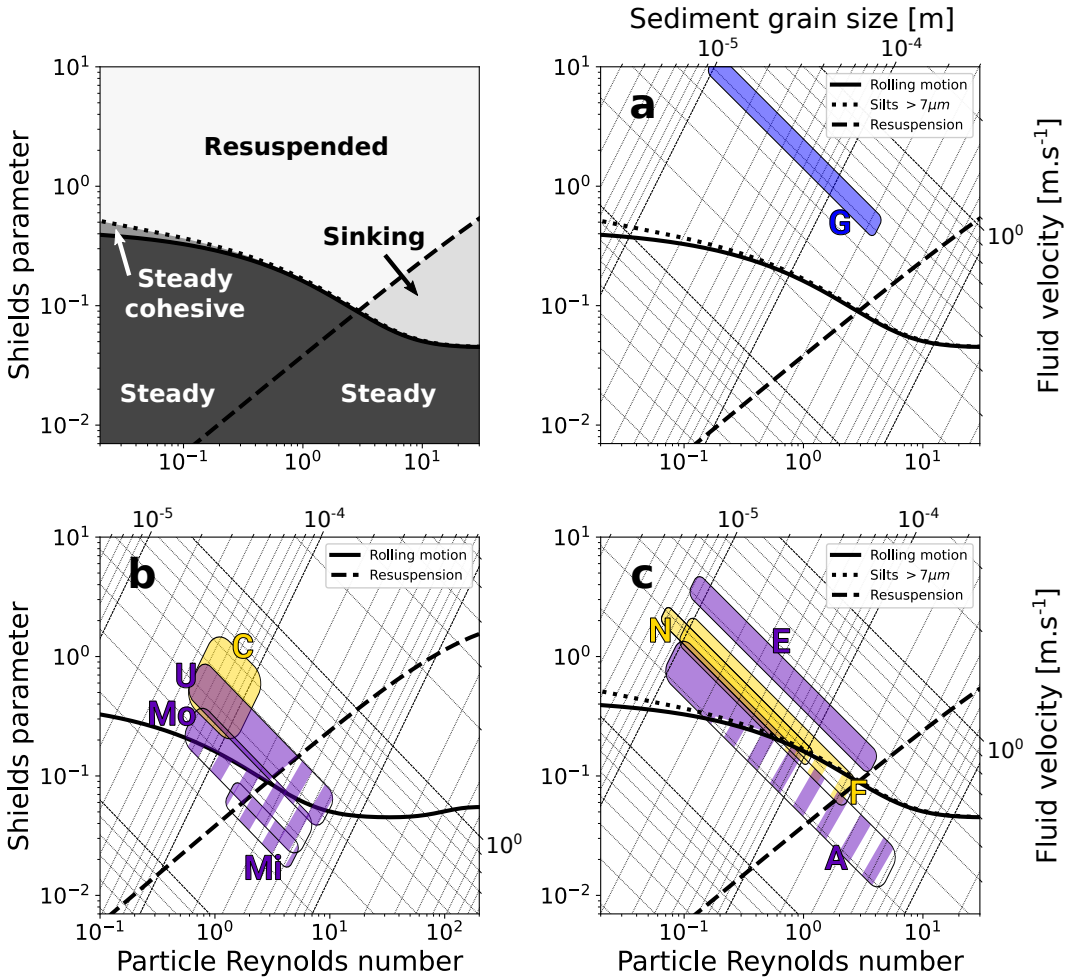

Figure 5. Sediment resuspension threshold for (a) silty light sediment TRSs, (b) dense sediment TRSs and (c) silty dense sediment TRSs. Above the solid line the sediment is lifted from the sea floor, above the dotted line the cohesive silts larger the 7 μm are lifted from the sea floor and above the dashed line the sediment stays in suspension. The colors denote the nature of the sediment: blue for biogenic, yellow for lithogenic, and purple for a mix of both. Hatched color highlights steady sediment. The grid scales of sediment grain size versus fluid velocity are computed for sea water properties ($\nu = 1.10^{-3}\ m^2.s^{-1}$, $\sigma = 27\ kg.m^{-3}$) for sediment density $\rho_S = 1.7\ g.cm^{-3}$ ((*e.g.* chalk) for (a) and $\rho_S = 2.5\ g.cm^{-3}$ (*e.g.* quartz, calcite) for (b,c).

Table 1. Characteristics of the potential tidal resuspension sites (TRS). The flow dynamics at the bottom come from the IT simulation and the sediment properties come from the cited literature. The intensity of the sediment resuspension is symbolized by ++ when all the sediment can be resuspended, + when only the smaller fraction can and **0** when any of it can.

Area	Criticality	Isopycnals $kg.m^{-3}$	τ_b $kg.m^{-1}.s^{-2}$	ρ_S $g.cm^{-3}$	D μm	Nature	References	TRS
C	Yes/No	27.0-28.2	0.20-0.52	2.5	50-100	Lit.	Flach et al. (2002)	++
F	Yes	27.0-28.2	0.14-0.16	2.5	10-200	Lit.	van Weering & de Stigter (1998)	+
U	Yes	27.1-27.8	0.11-0.26	2.5	50-600	Mix.	van Weering & de Stigter (1998)	+
G	Yes/No	27.5	0.55-0.70	1.7	10-200	Bio.	Flach et al. (2002) Yenes et al. (2019)	++
Mi	Yes	27.1-27.2	0.23	2.3	150-500	Mix.	Dias & Nittrouer (1984)	**0**
A	Yes/No	27.1-27.8	0.28	2.3	10-300	Mix.	Dias & Nittrouer (1984)	+
M	No	27.0-27.5	0.25	2.3	60-500	Mix.	Dias & Nittrouer (1984) Duarte & Taborda (2007)	+
N	Yes/No	27.4-27.8	0.41	2.5	7-30	Lit.	de Stigter et al. (2007) Ribeiro (2008)	+
E	Yes	27.1-27.9	0.41	2.5	8-120	Mix.	Balsinha (2020)	++

silt do not react the same as non-cohesive one so another curve is added for sediment with slits (Fig. 5a,c).

The Galicia Bank, La Coruña shelf and Estremadura Spur shelf are well above the threshold curve, suggesting that sediment resuspension occurs during the common tidal cycle. The Nazaré canyon and Fisterra shelf are mostly above the threshold curve, suggesting that only the finer fraction of the sediment is resuspended during the common tidal cycle and the medium fraction during spring tides. The Ulla, Aveiro and Mondego shelves are crossed by the threshold, so only the finer fraction of the sediment can be resuspended during spring tides. The Minho shelf is way below the threshold, so the sediment size is too large and the flow too slow to generate sediment resuspension.

This method gives us a first order estimation of the TRS along the Iberian peninsula. The Table 1 summarizes the isopycnals, the nature of the sediment, and the intensity of the resuspension at the investigated TRS.

4 Sediment transport

As reported in the introduction, the suspended particles seem to be transported as far as 2000 km offshore. However, IT transport of sediment only occurs over smaller scales (Masunaga et al., 2020, Molinas et al., 2020). In addition, ITs generated in the

area do not present a significant propagation pattern that would allow connecting the stations 1, 13 or 21 (Fig. 3a). Thus, we suggest that although ITs clearly trigger bottom friction and sediment resuspension, they are not responsible for the transport of suspended particles between the GEOVIDE stations; however, advection by the oceanic circulation may be. The IBIRYS operational reanalysis current field is used to investigate this transport. This product is a reanalysis from a 3D NEMO simulation at $1/12^o$: this simulation was assimilated with temperature and salinity profiles, sea surface height and sea surface temperature to better represent historical state of the ocean (further description and validation are provided by Maraldi et al., 2013). This simulation only extends to 19^oW and therefore, does not include station 21 of the GEOVIDE cruise. The daily averaged currents of IBIRYS are collocated with GEOVIDE measurements for comparison. The measurements and simulation results have been found to be in agreement, asserting the use of this simulation to investigate the regional circulation (Supporting Information Fig. S4).

The transport of the sediment by the circulation follow the isopycnals so IBIRYS have been interpolated at the isopycnals of the nepheloid layers observed: σ = 27.0, 27.17 and 27.39 $kg.m^{-3}$ (Fig. 1). With a velocity range of 3-10 $cm.s^{-1}$ and a distance between the TRS and the GEOVIDE stations of $\sim$ 500 km, the timescale involved ranges of 50-200 days. The monthly mean current field is averaged over 3 different time periods (2 years, 6 months and 3 months). For each period, the flow is considered steady and the streamlines are calculated to describe the potential pathways of the particles. When the shorter period is selected, a stronger mesoscale activity is observed with faster currents ($\sim$ 10 $cm.s^{-1}$), whereas slower currents ($\sim$ 3 $cm.s^{-1}$) are associated with the longer period. The sediment pathways from the TRS to the GEOVIDE stations slightly differ depending on the selected period; however, the general transport is clear. We choose to describe the sediment pathways using the 2-year average (from June 2012-June 2014) as it better shows a long-term mean state of the sediment transport (results based on the other periods are available in the Supporting Information Fig. S5).

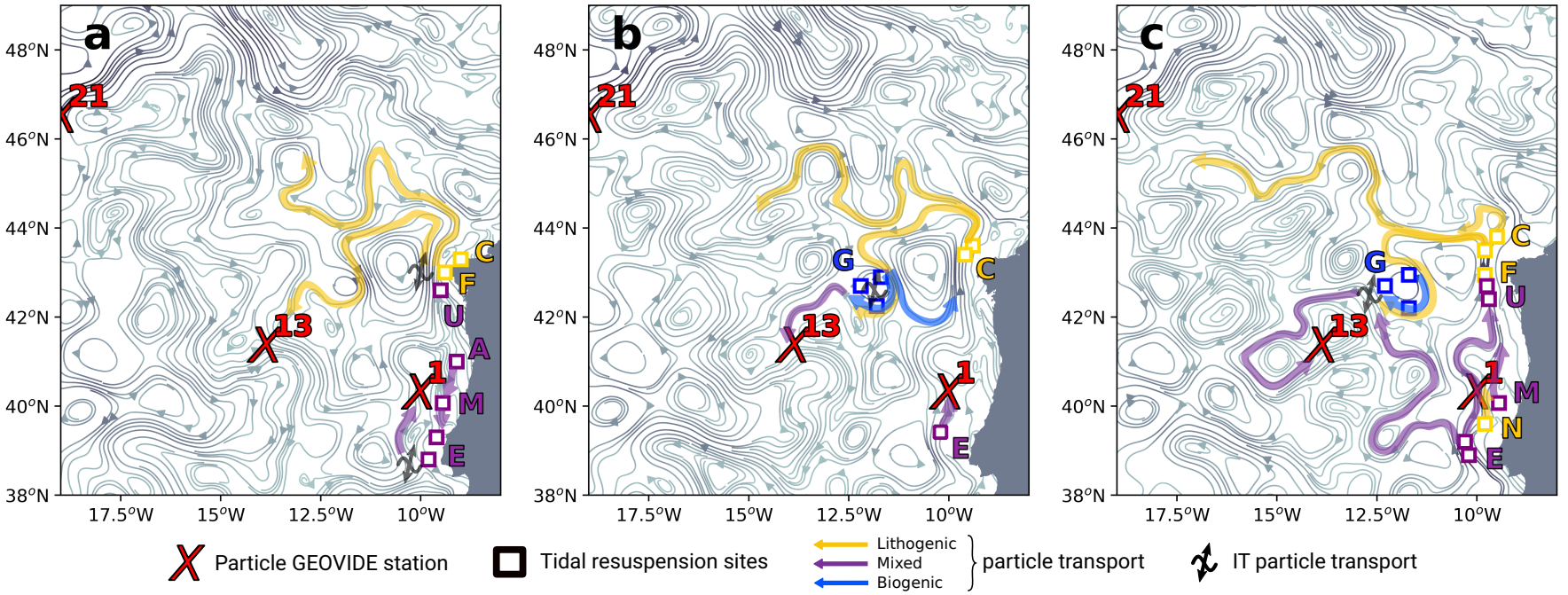

Figure 6. Streamline based on the mean velocity from June 2012 to June 2014 at (a) $\sigma = 27.0\ kg.m^{-3}$, (b) $\sigma = 27.17\ kg.m^{-3}$ and (c) $\sigma = 27.39\ kg.m^{-3}$. The arrows describe the potential pathways of the particles that may link the tidal resuspension sites and the GEOVIDE stations. The colors define the nature of the particles transported: yellow for lithogenic, blue for biogenic, and purple for both lithogenic and biogenic. The IT symbol refers to a situation where the particles are transported across streamlines by ITs.

Figure 6 presents the streamlines from velocity fields at each isopycnals. Note that the current structures at 27.0 $kg.m^{-3}$ (Fig. 6a) are consistent with the surface circulation during the cruise (Zunino et al., 2017, their figure 5, derived from altimetry sea level anomalies). Potential pathways from the TRS to the three GEOVIDE stations are inferred from the streamlines that connect them (colored arrows). The most striking feature is that no pathway directly connecting the three GEOVIDE stations is observed, at any isopycnal. A strong northward current along the shelf slope washes all the Iberian slope, then splits up in different directions at La Coruña shelf. The potential pathways between each station are described and discussed below.

Station 1 is influenced by two eddies: in front of the Aveiro shelf, the eddy structure is found at the three isopycnals, whereas in front of the Nazaré canyon, the eddy only affects the shallower one. The TRS potentially affecting station 1 vary depending on the isopycnal: at 27.0 $kg.m^{-3}$, Aveiro, Mondego and Estremadura Spur TRSs (purple arrows, Fig. 6a); at 27.17$kg.m^{-3}$, Estremadura Spur TRS (purple arrow, Fig. 6c); and at 27.39 $kg.m^{-3}$, Nazaré canyon and Estremadura Spur shef (yellow and purple arrows, Fig. 6c). With this method the station 1 seems mostly affected by mixed sediment so it can partially explain the lithogenic signature of the GEOVIDE observations. Note that some variations in the relative composition of the resuspended sediment cannot be excluded as well as other sediment coming from further south with the current as highlighted by Hernández-Molina et al. (2016).

Station 13 is mostly influenced by southward and northeastward currents; thus, the lithogenic particles observed at this station are transported following a circuitous pathway. This pathway is the same at every isopycnals: starting from the La Coruña TRS and circumventing the Galicia Bank (Fig. 6). At 27.0 $kg.m^{-3}$, this pathway transports particles mainly lithogenic from the La Coruña and Fisterra TRSs but also mixed sediment from Ulla TRS. At 27.17 $kg.m^{-3}$ and 27.39 $kg.m^{-3}$ however, the resuspension of biogenic sediment at the Galicia Bank can completely invert the ratio of lithogenic/biogenic particle within the suspended particles (blue and yellow to purple arrows, Fig. 6b,c). In addition, a current at 27.39$kg.m^{-3}$ seems to directly link Estremadura Spur TRS to station 13. Thus, we suggest that station 13 is affected by lithogenic particles for shallow isopycnals and mixed particles below. This is in good agreement with the GEOVIDE observations of lithogenic REEs (Fig. 1).

Some streamlines seem to hardly connect the TRSs and the GEOVIDE station, but could if ITs transport the particles across the streamline over 50-100 km (IT symbols in Fig. 6). This distance is comparable to that from the simulation of Masunaga et al. (2020), where the sediment is transported over 50 km by an IT flux of $\sim$ 5 $kW.m^{-1}$ (their figures 5 and 13). This could happen near La Coruña/Fisterra shelf, Galicia Bank and Estremadura Spur shelf where ITs energy flux $>$ 3 $kW.m^{-1}$ (Fig. 3a). As for station 1, currents may also bring sediment from areas further south (Hernández-Molina et al., 2016).

Station 21 does not seem to connect with the TRS at any isopycnal. Long and meandering pathways could approach station 21 from La Coruña but no further than 17^{o}W (yellow arrow, Fig. 6c). Moreover, a large northeastward current highly influences station 21: from $\sim$ 12 $cm.s^{-1}$ at 27.0 $kg.m^{-3}$ to 6 $cm.s^{-1}$ at 27.39 $kg.m^{-3}$. This current is one of the southern branches of the North Atlantic Current (SNAC) highlighted by Zunino et al. (2017). The authors show that station 21 is under the influence of a large anticyclonic eddy during the cruise. This station displays very different temperature and salinity than the nearby stations (Supporting Information Fig. S1), with Subpolar Mode Water below 180 m and Subarctic Intermediate Water at 500 m (Garcia-Ibanez et al., 2018). Current velocity across the GEOVIDE transect highlights a strong shear current centered on station 21. It cannot be excluded that this complex circulation could bring water masses from other coastal/shelf margin locations than the Iberian coast. For example, the East North Atlantic Central Waters

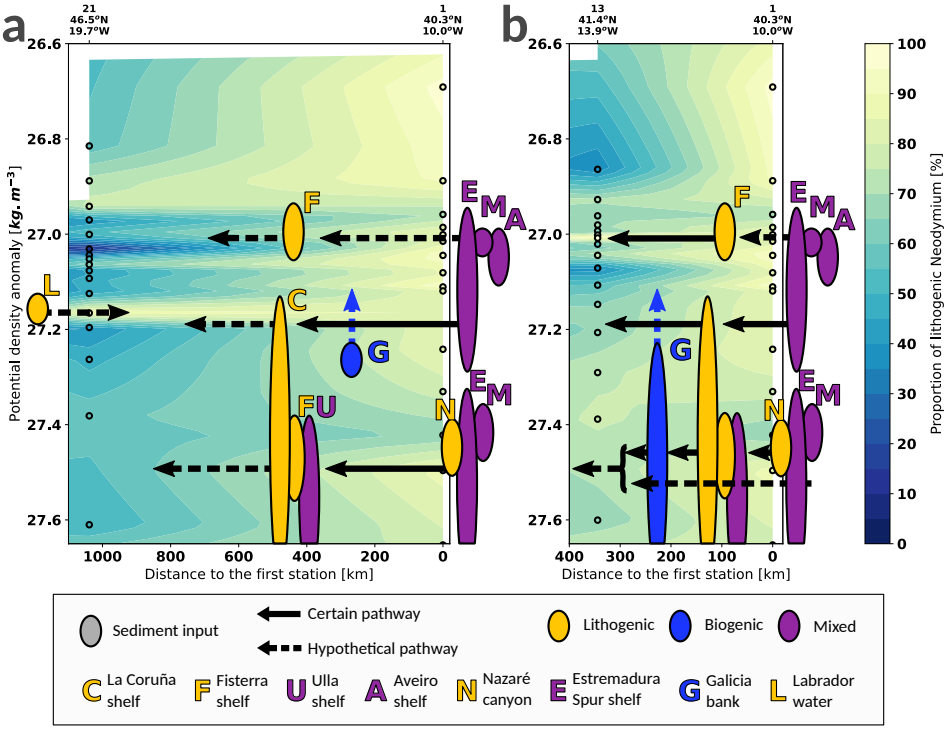

Figure 7. Proportion of lithogenic neodymium in particulate matter along isopycnals (a) between station 1 and 21 and (b) between station 1 and 13) using linear interpolation. The color inside the black rings refers to the GEOVIDE measurements. The other symbols refer to the tidal resuspension sites and the transport of the particles. On top of each station there is the station number and its localization. Data from Lagarde et al. (2020).

are highly represented at this depth (Garcia-Ibanez et al., 2018) and may have been influenced by ITs from the Gulf of Maine (Duda et al., 2018). The present choice of such regional model reanalysis does not enable us to reach a conclusion on the origins of the highly lithogenic particles observed at station 21. This will require further investigations based on a Lagrangian methodology (Maes & Blanke, 2015, Artigue et al., 2020) applied to a simulation of the North Atlantic basin reproducing the mixing of the various water masses in the North Atlantic and tidal dynamics. The ongoing study of neodymium isotopic composition (ϵNd) of the GEOVIDE samples could help to determine the exact origin of the particles (Grenier et al., 2018).

The simulation of the oceanic circulation provides a better understanding of the transport of the suspended particles over the area. Distinct pathways are highlighted for each station. Because stations 13 and 21 are not connected, the interpolation of the particulate lithogenic fraction between these two stations is not relevant and hampers the interpretation of the results. Distinct interpolations of the GEOVIDE measurements are proposed in Figure 7. The results shown in Table 1 and Figure 6 were added to the Figure 7 in order to propose a clear summary of our study.

5 Conclusion and perspectives

This study proposes the first interdisciplinary approach to explain the resuspension and transport of lithogenic particles from the Iberian coast to the middle of the North Atlantic basin. Based on a semi-realistic 3D tidal model and sediment proper-

ties, we establish that ITs generated in the Bay of Biscay and along the Iberian slope participate in sediment resuspension and could be the major mechanism for the resuspension occurring below 300 m. Eight TRS are identified: La Coruña shelf, Fisterra shelf and Nazaré canyon are sources of lithogenic sediment, the Ulla, Aviero, Mondego and Estremadura Spur shelves are likely providing both lithogenic and biogenic sediments, and the Galicia Bank is a source of biogenic sediment. Most of these sites are under strong IT influence, except some areas of Estremadura Spur shelf, strong bottom friction is only due to barotropic tidal currents at the top of the shelf slope. Using a regional model reanalysis, the mean state of the oceanic circulation in the area is investigated on the suspected isopycnals. Associated with the TRS, this approach explains most of the GEOVIDE observations (Lagarde et al., 2020). However, we demonstrate that stations 13 and 21 are not connected. More specifically, the significant lithogenic fraction and the water masses observed at station 21 at 500 m ($27.17\ kg.m^{-3}$) could reflect transport of sediment originating from the North American margins rather than from the Iberian margin.

More broadly, questions raised by the geochemical results lead to the development of this method associating dedicated IT simulation to regional circulation one. This strategy helped to improve the first interpretations of the geochemical data (Gourain et al., 2019, Lagarde et al., 2020). Not all TRS from this study are located on critical slopes, and many critical slopes of the Iberian peninsula are not associated with a TRS. Thus, we suggest that the slope criticality is not sufficient to properly identify TRS and should be reserved to internal solitary waves (in the upper 300 m). An explicit modeling of the ITs with a thin grid resolution ($< 3\ km$) and a good knowledge of the sediment properties (nature and size) are required to simulate and identify TRSs. Further work on sediment resuspension and large distance particle transport should consider applying Lagrangian tracking to the oceanic circulation simulations as well as performing a complete tidal-circulation model coupled with a sediment model.

Acknowledgments

The authors are grateful to the CNES, CLS, CNRS and UPS for the funding of this study. The authors are thankful to D. Allain for the development of the POCViP visualization software, to H. de Stigter, who provided us with the sediment properties near the Nazaré canyon, and to R. Almar for his advice on sediment resuspension.

The BOBIBE simulation was performed using HPC resources from GENCI/CINES (grants 2020-A0080110098 and 2021A0100110098). The GEOVIDE CTD data are available at SENOE (DOI: 10.17882/52153). The GEOVIDE geochemical tracer data, as part of GEOTRACE program, are provided by the British Oceanographic Data Centre (BODC), funded by the Scientific Committee on Oceanic Research, the US National Science Foundation and the UK Natural Environment Research Council (`https://www.bodc.ac.uk/geotraces/data/idp2017/`). The sediment properties from OMEX II-II project are provided by the BODC, funded by the European Commission through the Marine Science and Technology program (`https://www.bodc.ac.uk/omex/omexii-ii/`).

References

Arakawa, A., & Lamb, V. R. (1981). A potential enstrophy and energy conserving scheme for the shallow water equations. *Monthly Weather Review*, *109*(1), 18–36.

Artigue, L., Lacan, F., Van Gennip, S., Lohan, M. C., Wyatt, N. J., Woodward, E. M. S., ... Drillet, Y. (2020). Water mass analysis along 22 n in the subtropical north atlantic for the jc150 cruise (geotraces, gapr08). *Deep Sea Research Part I: Oceanographic Research Papers*, 103230.

Balsinha, M. J. (2020). *Sedimentary dynamics in the estremadura spur continental*

shelf (Unpublished doctoral dissertation). Universidade de Lisboa.

Boegman, L., & Stastna, M. (2019). Sediment resuspension and transport by internal solitary waves. *Annual Review of Fluid Mechanics*, *51*, 129–154.

Buijsman, M. C., Arbic, B. K., Richman, J. G., Shriver, J. F., Wallcraft, A. J., & Zamudio, L. (2017). Semidiurnal internal tide incoherence in the equatorial p acific. *Journal of Geophysical Research: Oceans*, *122*(7), 5286–5305.

Cacchione, D. (1970). *Experimental study of internal gravity waves over a slope* (Unpublished doctoral dissertation). Massachusetts Institute of Technology and Woods Hole Oceanographic Institution.

Cacchione, D., Pratson, L. F., & Ogston, A. (2002). The shaping of continental slopes by internal tides. *Science*, *296*(5568), 724–727.

Costa, A., Doglioli, A. M., Marsaleix, P., & Petrenko, A. A. (2017). Comparison of in situ microstructure measurements to different turbulence closure schemes in a 3-d numerical ocean circulation model. *Ocean Modelling*, *120*, 1–17.

Damien, P., Bosse, A., Testor, P., Marsaleix, P., & Estournel, C. (2017). Modeling postconvective submesoscale coherent vortices in the northwestern m editerranean s ea. *Journal of Geophysical Research: Oceans*, *122*(12), 9937–9961.

de Lavergne, C., Falahat, S., Madec, G., Roquet, F., Nycander, J., & Vic, C. (2019). Toward global maps of internal tide energy sinks. *Ocean Modelling*, *137*, 52–75.

de Madron, X. D., Castaing, P., Nyffeler, F., & Courp, T. (1999). Slope transport of suspended particulate matter on the aquitanian margin of the bay of biscay. *Deep Sea Research Part II: Topical Studies in Oceanography*, *46*(10), 2003–2027.

de Stigter, H. C., Boer, W., de Jesus Mendes, P. A., Jesus, C. C., Thomsen, L., van den Bergh, G. D., & van Weering, T. C. (2007). Recent sediment transport and deposition in the nazaré canyon, portuguese continental margin. *Marine Geology*, *246*(2-4), 144–164.

Dias, J., Jouanneau, J., Gonzalez, R., Araújo, M., Drago, T., Garcia, C., ... Weber, O. (2002). Present day sedimentary processes on the northern iberian shelf. *Progress in Oceanography*, *52*(2-4), 249–259.

Dias, J., & Nittrouer, C. A. (1984). Continental shelf sediments of northern portugal. *Continental Shelf Research*, *3*(2), 147–165.

Duarte, J. F., & Taborda, R. (2007). Bottom sediment signature associated with the oporto, aveiro and nazaré submarine canyons (nw off portugal). *Thalassas*, *23*(1), 9–18.

Duda, T. F., Lin, Y.-T., Buijsman, M., & Newhall, A. E. (2018). Internal tidal modal ray refraction and energy ducting in baroclinic gulf stream currents. *Journal of Physical Oceanography*, *48*(9), 1969–1993.

Estournel, C., Marsaleix, P., & Ulses, C. (2021). A new assessment of the circulation of atlantic and intermediate waters in the eastern mediterranean. *Progress in Oceanography*, *198*, 102673.

Flach, E., Muthumbi, A., & Heip, C. (2002). Meiofauna and macrofauna community structure in relation to sediment composition at the iberian margin compared to the goban spur (ne atlantic). *Progress in oceanography*, *52*(2-4), 433–457.

Garcia-Ibanez, M. I., Pérez, F. F., Lherminier, P., Zunino, P., Mercier, H., & Tréguer, P. (2018). Water mass distributions and transports for the 2014 geovide cruise in the north atlantic. *Biogeosciences*, *15*(7), 2075–2090.

Garrett, C., & Kunze, E. (2007). Internal tide generation in the deep ocean. *Annu. Rev. Fluid Mech.*, *39*, 57–87.

Gourain, A., Planquette, H., Cheize, M., Lemaitre, N., Menzel Barraqueta, J.-L., Shelley, R., ... Sarthou, G. (2019). Inputs and processes affecting the distribution of particulate iron in the north atlantic along the geovide (geotraces ga01) section. *Biogeosciences*, *16*(7), 1563–1582.

Grenier, M., Garcia-Solsona, E., Lemaitre, N., Trull, T. W., Bouvier, V., Nonnotte, P., ... Jeandel, C. (2018). Differentiating lithogenic supplies, water mass trans-

port, and biological processes on and off the kerguelen plateau using rare earth element concentrations and neodymium isotopic compositions. *Frontiers in Marine Science*, *5*, 426.

Griffies, S. M., & Hallberg, R. W. (2000). Biharmonic friction with a smagorinsky-like viscosity for use in large-scale eddy-permitting ocean models. *Monthly Weather Review*, *128*(8), 2935–2946.

Hernández-Molina, F. J., Wåhlin, A., Bruno, M., Ercilla, G., Llave, E., Serra, N., ... others (2016). Oceanographic processes and morphosedimentary products along the iberian margins: A new multidisciplinary approach. *Marine Geology*, *378*, 127–156.

Huthnance, J. (1989). Internal tides and waves near the continental shelf edge. *Geophysical & Astrophysical Fluid Dynamics*, *48*(1-3), 81–106.

Huthnance, J., Van Aken, H. M., White, M., Barton, E. D., Le Cann, B., Coelho, E. F., ... Vitorino, J. (2002). Ocean margin exchangewater flux estimates. *Journal of Marine Systems*, *32*(1-3), 107–137.

Jackett, D. R., McDougall, T. J., Feistel, R., Wright, D. G., & Griffies, S. M. (2006). Algorithms for density, potential temperature, conservative temperature, and the freezing temperature of seawater. *Journal of Atmospheric and Oceanic Technology*, *23*(12), 1709–1728.

Jia, Y., Tian, Z., Shi, X., Liu, J. P., Chen, J., Liu, X., ... Tian, J. (2019). Deep-sea sediment resuspension by internal solitary waves in the northern south china sea. *Scientific reports*, *9*(1), 1–8.

Kundu, P., Cohen, M. I., & Hu, H. H. (2004). *Fluid mechanics*. Amsterdam: Elsevier Academic Press.

Lagarde, M., Lemaitre, N., Planquette, H., Grenier, M., Belhadj, M., Lherminier, P., & Jeandel, C. (2020). Particulate rare earth element behavior in the north atlantic (geovide cruise). *Biogeosciences*.

Lam, P. J., Heller, M. I., Lerner, P. E., Moffett, J. W., & Buck, K. N. (2020). Unexpected source and transport of iron from the deep peru margin. *ACS Earth and Space Chemistry*, *4*(7), 977–992.

Larsen, L., Sternberg, R., Shi, N., Marsden, M., & Thomas, L. (1981). Field investigations of the threshold of grain motion by ocean waves and currents. *Marine Geology*, *42*(1-4), 105–132.

Leonard, B. P. (1979). A stable and accurate convective modelling procedure based on quadratic upstream interpolation. *Computer methods in applied mechanics and engineering*, *19*(1), 59–98.

Lyard, F. H., Allain, D. J., Cancet, M., Carrre, L., & Picot, N. (2021). Fes2014 global ocean tides atlas: design and performances. *Ocean Science Discussions*, *2021*, 140. Retrieved from `https://os.copernicus.org/preprints/os-2020-96/` doi: 10.5194/os-2020-96

Maes, C., & Blanke, B. (2015). Tracking the origins of plastic debris across the coral sea: A case study from the ouvéa island, new caledonia. *Marine pollution bulletin*, *97*(1), 160–168.

Maraldi, C., Chanut, J., Levier, B., Ayoub, N., Mey, P. D., Reffray, G., ... others (2013). Nemo on the shelf: assessment of the iberia–biscay–ireland configuration. *Ocean Science*, *9*(4), 745–771.

Marin, F. (2011). Solitons: Historical and physical introduction. In R. A. Meyers (Ed.), *Mathematics of complexity anddynamical systems* (pp. 1561–1575). New York, NY: Springer New York. Retrieved from `https://doi.org/10.1007/978-1-4614-1806-1_100` doi: 10.1007/978-1-4614-1806-1_100

Marsaleix, P., Auclair, F., & Estournel, C. (2006). Considerations on open boundary conditions for regional and coastal ocean models. *Journal of Atmospheric and Oceanic Technology*, *23*(11), 1604–1613.

Marsaleix, P., Auclair, F., & Estournel, C. (2009). Low-order pressure gradient

schemes in sigma coordinate models: The seamount test revisited. *Ocean Modelling*, *30*(2-3), 169–177.

Marsaleix, P., Auclair, F., Floor, J. W., Herrmann, M. J., Estournel, C., Pairaud, I., & Ulses, C. (2008). Energy conservation issues in sigma-coordinate free-surface ocean models. *Ocean Modelling*, *20*(1), 61–89.

Marsaleix, P., Michaud, H., & Estournel, C. (2019). 3d phase-resolved wave modelling with a non-hydrostatic ocean circulation model. *Ocean Modelling*, *136*, 28–50.

Masunaga, E., Arthur, R. S., Fringer, O. B., & Yamazaki, H. (2017). Sediment resuspension and the generation of intermediate nepheloid layers by shoaling internal bores. *Journal of Marine Systems*, *170*, 31–41.

Masunaga, E., Arthur, R. S., & Yamazaki, H. (2020). Baroclinic residual circulation and mass transport due to internal tides. *Journal of Geophysical Research: Oceans*, *125*(4), e2019JC015316.

McCave, I., & Hall, I. R. (2002). Turbidity of waters over the northwest iberian continental margin. *Progress in Oceanography*, *52*(2-4), 299–313.

Miedema, S. (2012a). Constructing the shields curve: Part a fundamentals of the sliding, rolling and lifting mechanisms for the entrainment of particles. *Journal of dredging engineering*, *12*(1), 1–49.

Miedema, S. (2012b). Constructing the shields curve. part b: Sensitivity analysis, exposure and protrusion levels settling velocity, shear stress and friction velocity, erosion flux and laminar main flow. *J. Dredging Eng*, *12*, 50–92.

Miedema, S. (2013). Constructing the shields curve: Part ccohesion by silt, hjulstrom, sundborg. In *International conference on offshore mechanics and arctic engineering* (Vol. 55409, p. V006T10A023).

Molinas, E., Carneiro, J. C., & Vinzon, S. (2020). Internal tides as a major process in amazon continental shelf fine sediment transport. *Marine Geology*, *430*, 106360.

Oliveira, A., Vitorino, J., Rodrigues, A., Jouanneau, J., Dias, J., & Weber, O. (2002). Nepheloid layer dynamics in the northern portuguese shelf. *Progress in Oceanography*, *52*(2-4), 195–213.

Pairaud, I. L., Auclair, F., Marsaleix, P., Lyard, F., & Pichon, A. (2010). Dynamics of the semi-diurnal and quarter-diurnal internal tides in the bay of biscay. part 2: Baroclinic tides. *Continental Shelf Research*, *30*(3-4), 253–269.

Pairaud, I. L., Lyard, F., Auclair, F., Letellier, T., & Marsaleix, P. (2008). Dynamics of the semi-diurnal and quarter-diurnal internal tides in the bay of biscay. part 1: Barotropic tides. *Continental Shelf Research*, *28*(10-11), 1294–1315.

Puig, P., Palanques, A., Guillén, J., & El Khatab, M. (2004). Role of internal waves in the generation of nepheloid layers on the northwestern alboran slope: implications for continental margin shaping. *Journal of Geophysical Research: Oceans*, *109*(C9).

Quaresma, L. S., Vitorino, J., Oliveira, A., & da Silva, J. (2007). Evidence of sediment resuspension by nonlinear internal waves on the western portuguese mid-shelf. *Marine geology*, *246*(2-4), 123–143.

Ribbe, J., & Holloway, P. E. (2001). A model of suspended sediment transport by internal tides. *Continental Shelf Research*, *21*(4), 395–422.

Ribeiro, M. (2008). Dinâmica sedimentar da cabeceira do canhão submarino da nazaré. *Faculdade de Ciências da Universidade de Lisboa*, 14.

Schmidt, S., Chou, L., & Hall, I. R. (2002). Particle residence times in surface waters over the north-western iberian margin: comparison of pre-upwelling and winter periods. *Journal of Marine Systems*, *32*(1-3), 3–11.

Shields, A. (1936). Anwendung der aehnlichkeitsmechanik und der turbulenzforschung auf die geschiebebewegung. *PhD Thesis Technical University Berlin*.

Siddorn, J., & Furner, R. (2013). An analytical stretching function that combines

the best attributes of geopotential and terrain-following vertical coordinates. *Ocean Modelling*, *66*, 1–13.

Toublanc, F., Ayoub, N., Lyard, F., Marsaleix, P., & Allain, D. (2018). Tidal downscaling from the open ocean to the coast: a new approach applied to the bay of biscay. *Ocean Modelling*, *124*, 16–32.

Van Weering, T. C., De Stigter, H., Boer, W., & De Haas, H. (2002). Recent sediment transport and accumulation on the nw iberian margin. *Progress in Oceanography*, *52*(2-4), 349–371.

van Weering, T. C., & de Stigter, H. C. (1998). *Benthic boundary layer forcing on iberian margin particle fluxes and accumulation* (Tech. Rep.). OMEX II-II Second Annual Science Report. Retrieved from `https://www.bodc.ac.uk/omex/omexii-ii/report/05a_sr.pdf`

Yenes, M., Casas, D., Nespereira, J., Monterrubio, S., Ercilla, G., & López-González, N. (2019). Galicia bank sediment transport activity in response to continuous sedimentary instability dynamics: a geotechnical perspective. *International Journal of Earth Sciences*, *108*(8), 2545–2560.

Zaron, E. D. (2019). Baroclinic tidal sea level from exact-repeat mission altimetry. *Journal of Physical Oceanography*, *49*(1), 193-210. Retrieved from `https://doi.org/10.1175/JPO-D-18-0127.1` doi: 10.1175/JPO-D-18-0127.1

Zunino, P., Lherminier, P., Mercier, H., Daniault, N., García-Ibáñez, M. I., & Pérez, F. F. (2017). The GEOVIDE cruise in may–june 2014 reveals an intense meridional overturning circulation over a cold and fresh subpolar north atlantic. *Biogeosciences*, *14*(23), 5323–5342. doi: 10.5194/bg-14-5323-2017

Supporting Information for "Internal tides responsible for lithogenic inputs along the Iberian continental slope"

Simon Barbot[1], Marion Lagarde[1], Florent Lyard[1], Patrick Marsaleix[1],

Pascale Lherminier[2], Catherine Jeandel[1]

[1]LEGOS, Université de Toulouse, CNES, CNRS, IRD, UPS, Toulouse, France

[2]LOPS, Ifremer, Univ. Brest, CNRS, IRD, IUEM, Plouzané, France

Contents of this file

Introduction

Text S1 details the methodology for the calculation of the slope criticality. Text S2 details the feature used by the hydrodynamic numerical model SYMPHONIE and the specific choices that have been made for the BOBIBE configuration of this study. Figures S2 and S3 show validation of the barotropic and baroclinic tides for all the tidal harmonics used in the BOBIBE simulation. Figure S4 shows the validation of the IBIRYS12 reanalysis compared to GEOVIDE transect over co-located stations. Figure S5 details the impact of the average period used for the circulation to investigate the sediment transport. Table S1 lists the numerical and physical constants used for the BOBIBE configuration.

Text S1. Calculation of the slope criticality

The calculation of the critical slope is based on the ratio between the topography slope γ and the IT wave beam slope l. If $\gamma/c > 1$, the slope is considered as steep. If $\gamma/c > 1$, the slope is considered as flat. If $\gamma/c = 1$, the slope is considered as critical. The expression of c can be found from the dispersion relationship of the internal gravity wave in a rotating fluid (Kundu et al., 2004):

$$\omega^2 - N^2 \frac{k_H^2}{k_H^2 + k_V^2} + f^2 \frac{k_V^2}{k_H^2 + k_V^2} = 0 \tag{1}$$

with ω the wave frequency, N the Brunt-Vissl frequency, f the Coriolis parameter, k_H the horizontal wavenumber and k_V the vertical wavenumber. N is defined by the potential density profile:

$$N^2 = -\frac{g}{\rho_0} \frac{d\rho_0}{dz} \tag{2}$$

with g the gravitational acceleration, ρ_0 the unperturbed potential density. So for a given density profile, the IT wave beam slope can be calculated as the ratio between horizontal and vertical wavenumber:

$$c^2 = \frac{k_H^2}{k_V^2} = \frac{\omega^2 - f^2}{N^2 - \omega^2} \tag{3}$$

The calculation is made for M2, the dominant semi-diurnal tidal waves in this region. The diurnal tidal waves have no relevant criticality slope in this area because located outside the critical latitude ($f \geq \omega$).

Text S2. Numerical details of SYMPHONIE for the BOBIBE configuration

The numerical model SYMPHONIE[1] (Marsaleix et al., 2008, 2019) is based on the Navier-Stokes primitive equations solved on an Arakawa curvilinear C-grid (Arakawa & Lamb, 1981) under the hydrostatic and Boussinesq approximations. The model makes use of an energy conserving finite difference method described by Marsaleix et al. (2008), a forward-backward time stepping scheme, a Jacobian pressure gradient scheme (Marsaleix et al., 2009), the equation of state of Jackett, McDougall, Feistel, Wright, and Griffies (2006), and the K-epsilon turbulence scheme with the implementation described in Costa, Doglioli, Marsaleix, and Petrenko (2017). Horizontal advection and diffusion of tracers are computed using the QUICKEST scheme (Leonard, 1979) and vertical advection using a centered scheme. Horizontal advection and diffusion of momentum are each computed with a fourth order centered biharmonic scheme as in Damien, Bosse, Testor, Marsaleix, and Estournel (2017). The biharmonic viscosity of momentum is calculated according to a Smagorinsky-like formulation derived from Griffies and Hallberg (2000). The lateral open boundary conditions, based on radiation conditions combined with nudging conditions, are described in Marsaleix, Auclair, and Estournel (2006) and Toublanc, Ayoub, Lyard, Marsaleix, and Allain (2018).

The VQS (vanishing quasi-sigma) vertical coordinate described in Estournel, Marsaleix, and Ulses (2021) is used to avoid an excess of vertical levels in very shallow areas while maintaining an accurate description of the bathymetry and reducing the truncation errors associated with the sigma coordinate (Siddorn & Furner, 2013). The implementation of the tide, described in Pairaud, Lyard, Auclair, Letellier, and Marsaleix (2008); Pairaud, Auclair, Marsaleix, Lyard, and Pichon (2010), consists on the one hand of the amplitude

and phase of the tide introduced at the open lateral boundaries and on the other hand of the astronomical plus loading and self-attraction potentials.

In addition to this usual configuration of the model, specific nudging conditions have been developed for this particular study. To prevent the erosion of the stratification by the tides, a nudging term have been add in every point of the grid to maintain the initial value of temperature and salinity:

$$\frac{\partial X'}{\partial t} = ... + \lambda^R \bar{X}' \tag{4}$$

where X is the anomaly of either the temperature or the salinity, λ^R is the nudging frequency and X' is the difference to a reference field X_{ref} ($X' = X_{ref} - X$). The horizontal bar indicates a temporal filter that selects the low frequencies, so that gravity waves (considered high frequencies) are not damped by the nudging. The temporal filter is calculated by:

$$\frac{\partial \bar{X}'}{\partial t} = \lambda^{LF} \left(X_{ref} - X - \bar{X}' \right) \tag{5}$$

with the following numeric scheme:

$$\bar{X}'(t + \Delta t) = \left(1 - \Delta t \lambda^{LF}\right) \bar{X}'(t) + \Delta t \lambda^{LF} \left(X_{ref}(t) - X(t) \right) \tag{6}$$

whose filtering properties are detailed in Grebenkov and Serror (2014). Note that the possibility of oscillations during the transient solution produced by the coupling of Eq. 4 and Eq. 5 is eliminated by the following condition on λ^R:

$$\lambda^R = 0 \qquad if X' \bar{X}' < 0 \tag{7}$$

Otherwise, the value for λ^{relax}, λ^R and λ^{LF} are constant parameters and can be found in the Table S1.

References

Arakawa, A., & Lamb, V. R. (1981). A potential enstrophy and energy conserving scheme for the shallow water equations. *Monthly Weather Review*, *109*(1), 18–36.

Costa, A., Doglioli, A. M., Marsaleix, P., & Petrenko, A. A. (2017). Comparison of in situ microstructure measurements to different turbulence closure schemes in a 3-d numerical ocean circulation model. *Ocean Modelling*, *120*, 1–17.

Damien, P., Bosse, A., Testor, P., Marsaleix, P., & Estournel, C. (2017). Modeling postconvective submesoscale coherent vortices in the northwestern m editerranean s ea. *Journal of Geophysical Research: Oceans*, *122*(12), 9937–9961.

Estournel, C., Marsaleix, P., & Ulses, C. (2021). A new assessment of the circulation of atlantic and intermediate waters in the eastern mediterranean. *Progress in Oceanography*, *198*, 102673.

Grebenkov, D. S., & Serror, J. (2014). Following a trend with an exponential moving average: Analytical results for a gaussian model. *Physica A: Statistical Mechanics and its Applications*, *394*, 288–303.

Griffies, S. M., & Hallberg, R. W. (2000). Biharmonic friction with a smagorinsky-like viscosity for use in large-scale eddy-permitting ocean models. *Monthly Weather Review*, *128*(8), 2935–2946.

Jackett, D. R., McDougall, T. J., Feistel, R., Wright, D. G., & Griffies, S. M. (2006). Algorithms for density, potential temperature, conservative temperature, and the freezing temperature of seawater. *Journal of Atmospheric and Oceanic Technology*, *23*(12), 1709–1728.

Kundu, P., Cohen, M. I., & Hu, H. H. (2004). *Fluid mechanics*. Amsterdam: Elsevier

Academic Press.

Leonard, B. P. (1979). A stable and accurate convective modelling procedure based on quadratic upstream interpolation. *Computer methods in applied mechanics and engineering*, *19*(1), 59–98.

Lyard, F. H., Allain, D. J., Cancet, M., Carrre, L., & Picot, N. (2021). Fes2014 global ocean tides atlas: design and performances. *Ocean Science Discussions*, *2021*, 140. Retrieved from `https://os.copernicus.org/preprints/os-2020-96/` doi: 10 .5194/os-2020-96

Marsaleix, P., Auclair, F., & Estournel, C. (2006). Considerations on open boundary conditions for regional and coastal ocean models. *Journal of Atmospheric and Oceanic Technology*, *23*(11), 1604–1613.

Marsaleix, P., Auclair, F., & Estournel, C. (2009). Low-order pressure gradient schemes in sigma coordinate models: The seamount test revisited. *Ocean Modelling*, *30*(2-3), 169–177.

Marsaleix, P., Auclair, F., Floor, J. W., Herrmann, M. J., Estournel, C., Pairaud, I., & Ulses, C. (2008). Energy conservation issues in sigma-coordinate free-surface ocean models. *Ocean Modelling*, *20*(1), 61–89.

Marsaleix, P., Michaud, H., & Estournel, C. (2019). 3d phase-resolved wave modelling with a non-hydrostatic ocean circulation model. *Ocean Modelling*, *136*, 28–50.

Pairaud, I. L., Auclair, F., Marsaleix, P., Lyard, F., & Pichon, A. (2010). Dynamics of the semi-diurnal and quarter-diurnal internal tides in the bay of biscay. part 2: Baroclinic tides. *Continental Shelf Research*, *30*(3-4), 253–269.

Pairaud, I. L., Lyard, F., Auclair, F., Letellier, T., & Marsaleix, P. (2008). Dynamics

of the semi-diurnal and quarter-diurnal internal tides in the bay of biscay. part 1: Barotropic tides. *Continental Shelf Research*, *28*(10-11), 1294–1315.

Siddorn, J., & Furner, R. (2013). An analytical stretching function that combines the best attributes of geopotential and terrain-following vertical coordinates. *Ocean Modelling*, *66*, 1–13.

Toublanc, F., Ayoub, N., Lyard, F., Marsaleix, P., & Allain, D. (2018). Tidal downscaling from the open ocean to the coast: a new approach applied to the bay of biscay. *Ocean Modelling*, *124*, 16–32.

Zaron, E. D. (2019). Baroclinic tidal sea level from exact-repeat mission altimetry. *Journal of Physical Oceanography*, *49*(1), 193-210. Retrieved from `https://doi.org/10.1175/JPO-D-18-0127.1` doi: 10.1175/JPO-D-18-0127.1

Zunino, P., Lherminier, P., Mercier, H., Daniault, N., García-Ibáñez, M. I., & Pérez, F. F. (2017). The GEOVIDE cruise in may–june 2014 reveals an intense meridional overturning circulation over a cold and fresh subpolar north atlantic. *Biogeosciences*, *14*(23), 5323–5342. doi: 10.5194/bg-14-5323-2017

Notes

1. available at `https://sites.google.com/view/symphonieoceanmodel/home`

Table S1. Numerical and physical constants used in SYMPHONIE. As the spatial resolution is the same for longitude and latitude, only one of them is described.

Name	Symbol	Value
Internal time step	Δt	90 s
External time step	Δt_{ext}	1.25 s
Mean spatial step	$\bar{\Delta x}$	900 m
Minimum spatial step	Δx_{min}	800 m
Maximum spatial step	Δx_{max}	1000 m
Number of layers	nz	60
Size of the sponge layer	D_{sponge}	70 grid nodes
Boundary nudging frequency for velocity	λ^{relax}	0.1 days
Nudging frequency for T,S	λ^{R}	2 days
Low frequency for nudging	λ^{LF}	10 days
Bottom roughness	z_0^b	1×10^{-3} m
Minimum friction coefficient	$C_{D\,min}$	2.5×10^{-3}

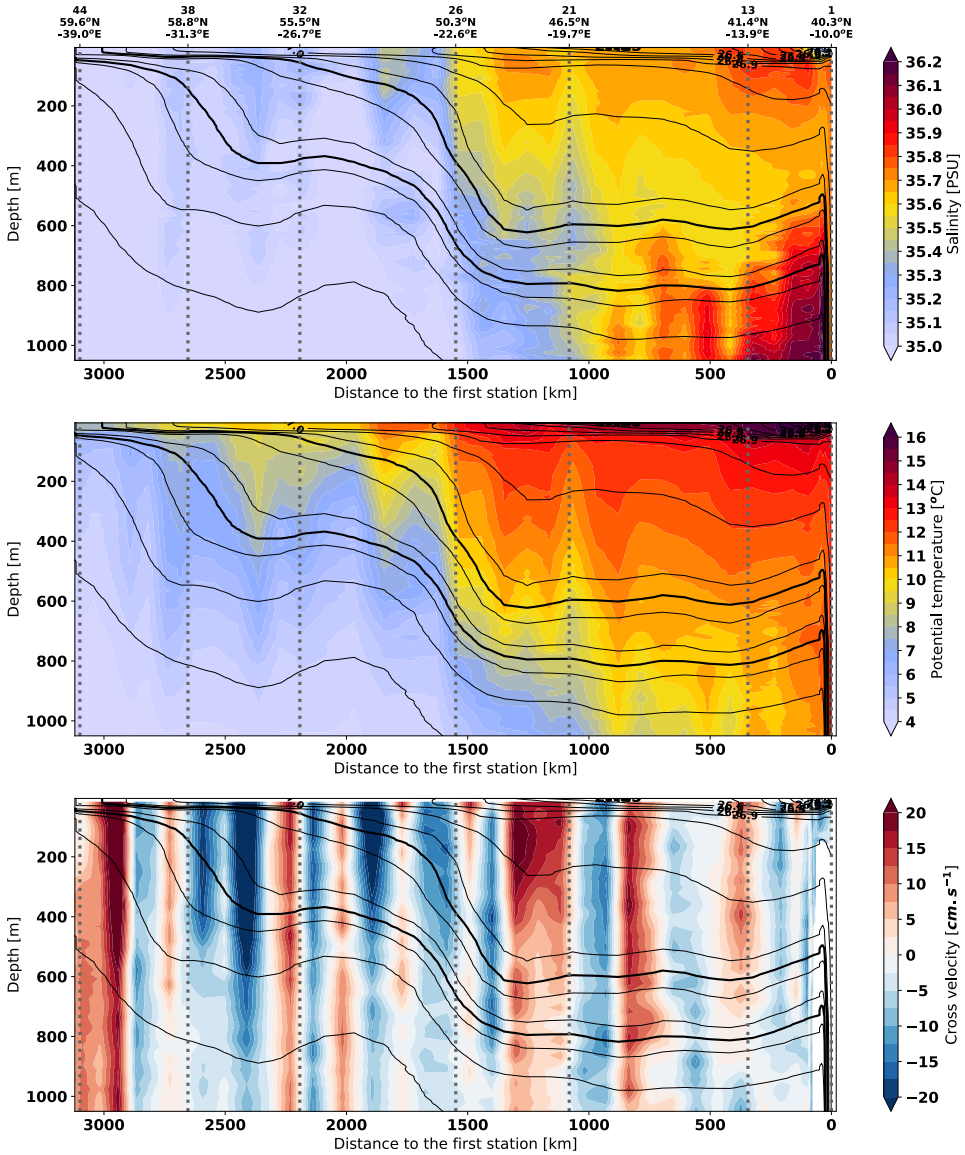

Figure S1. GEOVIDE measurements of (upper panel) the salinity, (central panel) the potential temperature and (lower panel) the velocity across the section from LADCP. The black lines represent the isopycnals of potential density anomaly. Each station where particles were sampled are represented by the dotted gray lines (station number and localization on top). Data from Zunino et al. (2017).

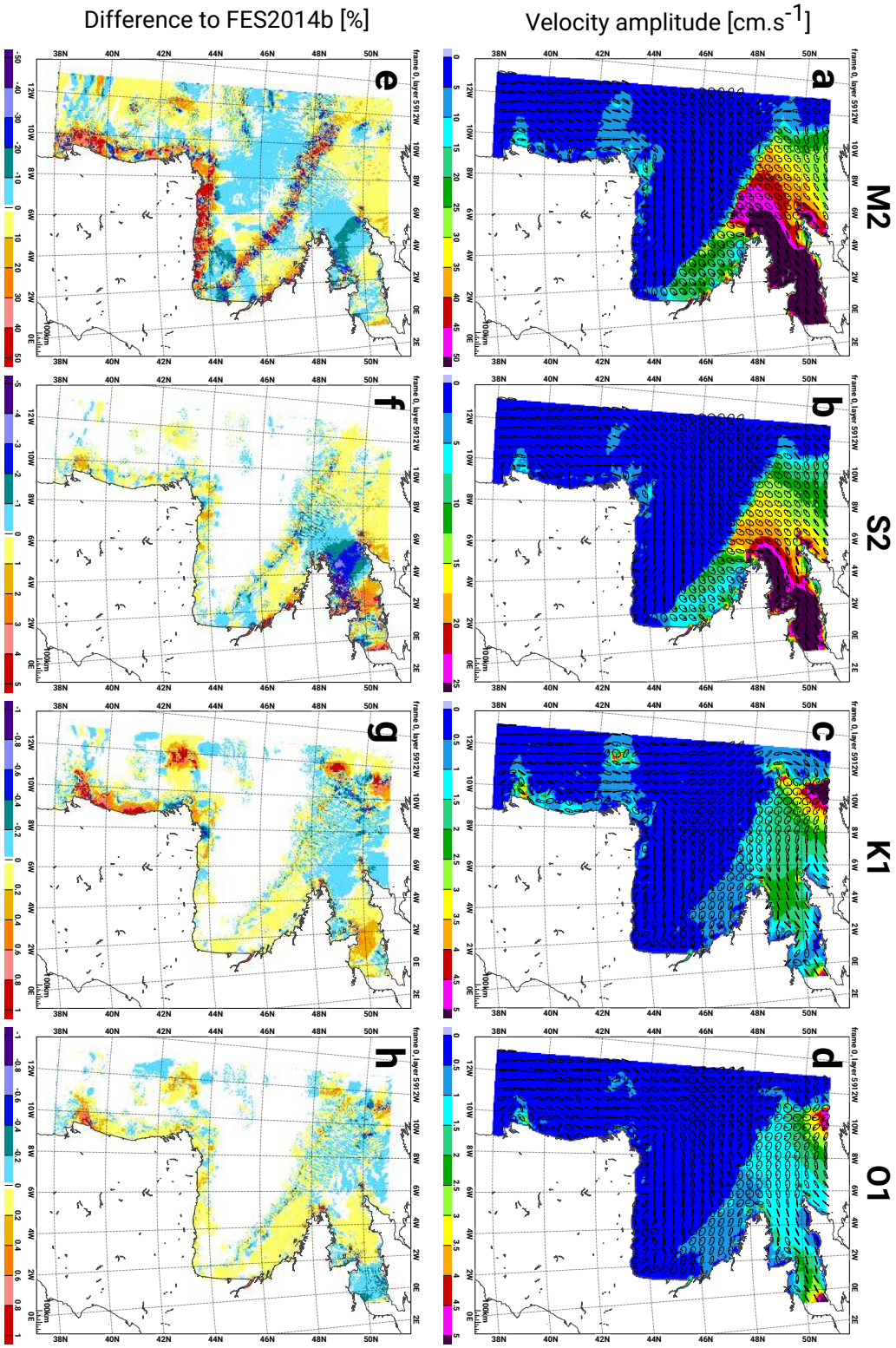

Figure S2. (a-e) Barotropic velocity amplitude for the simulated tidal harmonics and (f-j) the difference to FES2014b atlas (Lyard et al., 2021).

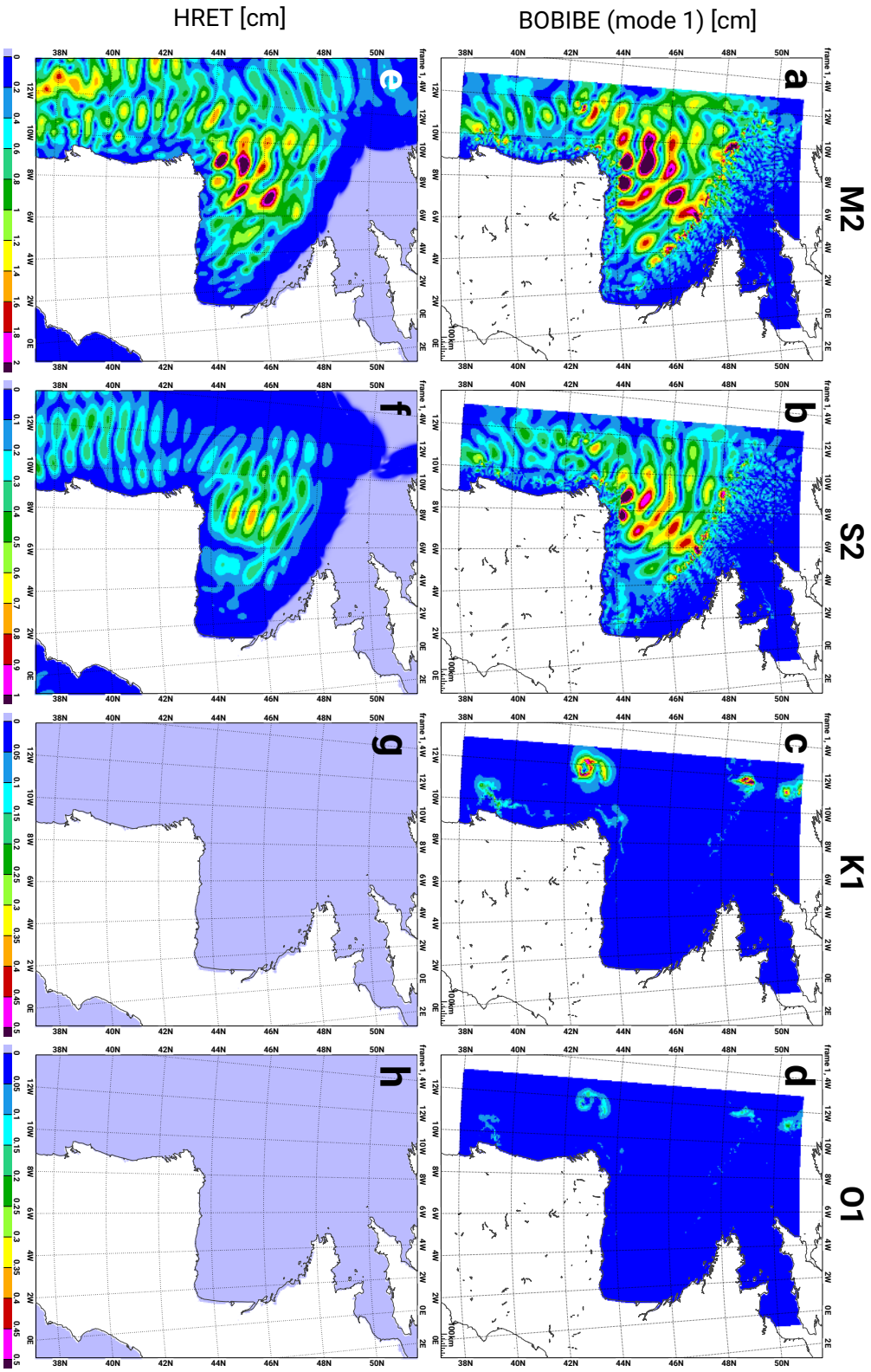

Figure S3. (a-d) Internal tide surface elevation amplitude for M2, S2, K1, O1 simulated tidal harmonics and (e-h) the corresponding value from HRET empirical IT atlas (Zaron, 2019).

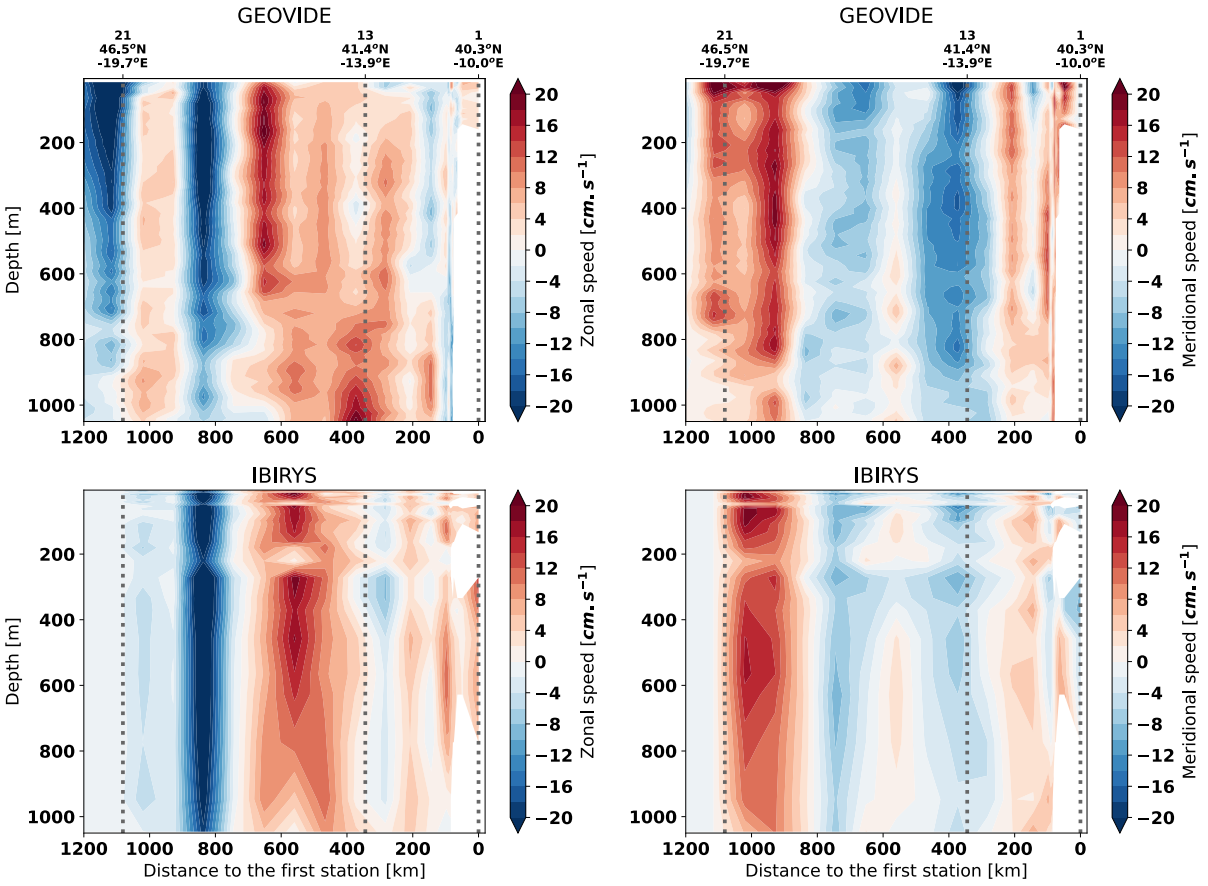

Figure S4. Vertical structure of the currents in the daily mean of IBIRYS12 reanalysis and GEOVIDE measurements. The values of IBIRYS12 are co-located (time and space) with the stations of the GEOVIDE cruise. GEOVIDE measurements from Zunino et al. (2017).

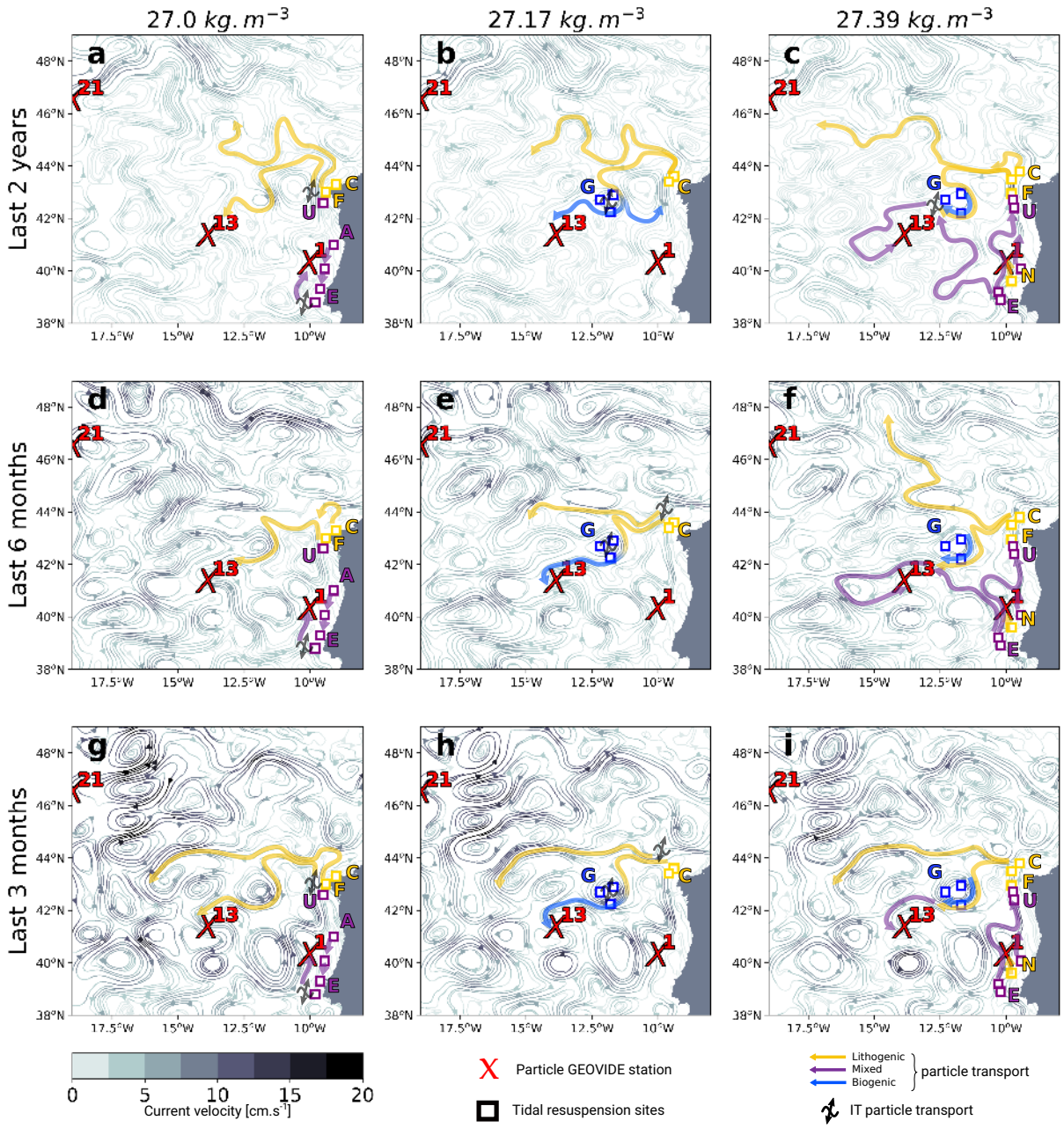

Figure S5. Streamline based on the mean velocity (top) 2 years, (center) 6 months and (bottom) 3 months before June 2014 at (left) 180 m, (middle) 500 m and 800 m. The red crosses show the GEOVIDE particle measurement stations. The squares show the location of tidal resuspension sites. The arrows describe the potential pathways of the particles from the tidal resuspension sites to the GEOVIDE stations. The colors define the nature of the particles transported: yellow for lithogenic, blue for biogenic and purple for both mixed.